In-medium similarity renormalization group with three-body operators

M. Heinz,[1,2,*] A. Tichai,[1,2,3,†] J. Hoppe,[1,2,‡] K. Hebeler,[1,2,§] and A. Schwenk[1,2,3,¶]

[1]*Technische Universität Darmstadt, Department of Physics, 64289 Darmstadt, Germany*
[2]*ExtreMe Matter Institute EMMI, GSI Helmholtzzentrum für Schwerionenforschung GmbH, 64291 Darmstadt, Germany*
[3]*Max-Planck-Institut für Kernphysik, Saupfercheckweg 1, 69117 Heidelberg, Germany*

Over the past decade the in-medium similarity renormalization group (IMSRG) approach has proven to be a powerful and versatile *ab initio* many-body method for studying medium-mass nuclei. So far, the IMSRG was limited to the approximation in which only up to two-body operators are incorporated in the renormalization group flow, referred to as the IMSRG(2). In this work, we extend the IMSRG(2) approach to fully include three-body operators yielding the IMSRG(3) approximation. We use a perturbative scaling analysis to estimate the importance of individual terms in this approximation and introduce truncations that aim to approximate the IMSRG(3) at a lower computational cost. The IMSRG(3) is systematically benchmarked for different nuclear Hamiltonians for ^{4}He and ^{16}O in small model spaces. The IMSRG(3) systematically improves over the IMSRG(2) relative to exact results. Approximate IMSRG(3) truncations constructed based on computational cost are able to reproduce much of the systematic improvement offered by the full IMSRG(3). We also find that the approximate IMSRG(3) truncations behave consistently with expectations from our perturbative analysis, indicating that this strategy may also be used to systematically approximate the IMSRG(3).

arXiv:2102.11172v3 [nucl-th] 26 Apr 2021

I. INTRODUCTION

A key challenge in nuclear structure theory is the calculation of the properties of atomic nuclei with predictive power extending to unmeasured, exotic systems targeted by modern rare-isotope facilities. *Ab initio* many-body approaches seek to accomplish this by solving the many-body Schrödinger equation in a systematically improvable manner using two- and three-body nuclear interactions as input. The rapid growth of the range of systems within reach of *ab initio* many-body methods over the past two decades [1–3] can be understood in terms of improvements in the input interactions [4–11] and improvements in many-body approaches for medium-mass nuclei.

To access medium-mass and heavier systems, the many-body approaches used in *ab initio* calculations start from an A-body reference state on which corrections are systematically constructed. These methods scale polynomially in the size of the computational basis N rather than exponentially in the number of particles A, as is the case for the exact solution of the A-body Schrödinger equation. Examples of such methods are coupled-cluster (CC) theory [12, 13], the in-medium similarity renormalization group (IMSRG) [14–16], self-consistent Green's function (SCGF) theory [17, 18], and many-body perturbation theory (MBPT) [19–22]. These methods all share a many-body truncation that can be systematically relaxed and in the limit of no many-body truncation recover the exact results.

In this work, we focus on the systematic improvement of the IMSRG, which is currently truncated at the normal-ordered two-body level, the IMSRG(2) approximation. In coupled-cluster theory, many different methods have been developed to approximately and exactly handle three-body effects in many-body calculations [12, 23–28]. These effects have been shown to be important for the reproduction of a range of observables, such as 2^+ excited-state energies at closed shells [29], dipole polarizabilities [30, 31], and nuclear β-decay matrix elements [32]. In these cases, the IMSRG(2) performance is deficient relative to methods that are able to treat three-body effects [33]. For the IMSRG, truncations that include induced three-body effects have been applied to shell-model diagonalizations using universal shell-model interactions [34]. In quantum chemistry, the driven similarity renormalization group, a similar many-body method to the IMSRG, has been extended to approximately include three-body effects in ways designed to reproduce the success of coupled-cluster theory in electronic systems [35]. For the IMSRG, however, studies of the role of three-body operators for nuclear systems have not yet been performed.

To systematically study three-body operators in the IMSRG, we extend the many-body truncation to the normal-ordered three-body level, defined as the IMSRG(3) approximation, and construct various different approximate IMSRG(3) truncation schemes with reduced computational cost. We apply these truncation schemes to closed-shell systems in small model spaces and analyze their properties in detail using perturbative tools. We study how they compare to exact results obtained from full diagonalizations, analyze the systematics of the many-body expansion in these systems, and investigate how full IMSRG(3) results can be approximated at a lower computational cost.

In Sec. II, we give an overview of the IMSRG formalism. Section III discusses the IMSRG(3) truncation, provides the fundamental commutators for the truncation, gives an overview of the perturbative analysis to understand their relative importance, and introduces approximate IMSRG(3) truncation schemes. In Sec. IV, we apply the IMSRG(3) and our approximate truncation schemes to the closed-shell nuclei ^{4}He and ^{16}O. Finally, we summarize our results in Sec. V.

* mheinz@theorie.ikp.physik.tu-darmstadt.de
† alexander.tichai@physik.tu-darmstadt.de
‡ jhoppe@theorie.ikp.physik.tu-darmstadt.de
§ kai.hebeler@physik.tu-darmstadt.de
¶ schwenk@physik.tu-darmstadt.de

II. MANY-BODY FORMALISM

A. Operator representation

In this work, an A-body operator

$$O = O^{(0)} + \cdots + O^{(A)} \tag{1}$$

is composed of zero- through A-body parts, given in second-quantized form by

$$O^{(A)} = \frac{1}{(A!)^2} \sum_{p_1,\ldots,p_{2A}} O_{p_1\cdots p_{2A}} a^\dagger_{p_1} \cdots a^\dagger_{p_A} a_{p_{2A}} \cdots a_{p_{A+1}} \tag{2}$$

with the antisymmetrized matrix elements $O_{p_1\cdots p_{2A}}$ and the fermion creation (annihilation) operators $a^\dagger_p$ (a_p), which create (annihilate) a particle in the single-particle state $|p\rangle$.

Normal-ordering techniques can be used to exactly rearrange O into normal-ordered zero- through A-body parts,

$$O = \tilde{O}^{(0)} + \cdots + \tilde{O}^{(A)}, \tag{3}$$

where the normal ordering is performed with respect to a reference state that is a good starting approximation for the targeted ground or excited state. The normal-ordered A-body parts are given by

$$\tilde{O}^{(A)} = \frac{1}{(A!)^2} \sum_{p_1,\ldots,p_{2A}} \tilde{O}_{p_1\cdots p_{2A}} : a^\dagger_{p_1} \cdots a^\dagger_{p_A} a_{p_{2A}} \cdots a_{p_{A+1}} : . \tag{4}$$

In Eqs. (3) and (4), the tilde distinguishes the normal-ordered operator and its normal-ordered matrix elements from their free-space equivalents in Eqs. (1) and (2). The normal ordering of the string of creation and annihilation operators is indicated by the surrounding colons, $: \cdots :$. In the following, we work exclusively with normal-ordered operators and matrix elements and leave the tilde off to simplify notation.

We focus on the case where the reference state to describe an A-body system is a single A-particle Slater determinant:

$$|\Phi\rangle = \prod_{i=1}^{A} a^\dagger_{p_i} |0\rangle , \tag{5}$$

where $|0\rangle$ is the vacuum, the state where no particles are present. For a single-particle state $|p\rangle$, if it is occupied in the reference state, then it has occupation number $n_p = 1$ and is called a hole state. Similarly, if it is unoccupied in the reference state, then it has $n_p = 0$ and is called a particle state. The A-body Hilbert space is spanned by the reference state and its elementary excitations

$$|\Phi^{a_1\cdots a_B}_{i_1\cdots i_B}\rangle = a^\dagger_{a_B} \cdots a^\dagger_{a_1} a_{i_B} \cdots a_{i_1} |\Phi\rangle , \tag{6}$$

which can be constructed by exciting the fermions in the hole states $|i_1\rangle$ through $|i_B\rangle$ into the particle states $|a_1\rangle$ through $|a_B\rangle$. This state is a B-particle B-hole ($BpBh$) excited state, where $B \leq A$.

A conventional notation for the normal-ordered Hamiltonian is

$$H = E + f + \Gamma + W \tag{7}$$

$$\begin{aligned} &= E + \sum_{pq} f_{pq} : a^\dagger_p a_q : + \frac{1}{(2!)^2} \sum_{pqrs} \Gamma_{pqrs} : a^\dagger_p a^\dagger_q a_s a_r : \\ &\quad + \frac{1}{(3!)^2} \sum_{pqrstu} W_{pqrstu} : a^\dagger_p a^\dagger_q a^\dagger_r a_u a_t a_s : , \end{aligned} \tag{8}$$

where E is the reference-state expectation value of the Hamiltonian, $\langle\Phi|H|\Phi\rangle$, and f, Γ, and W are the normal-ordered one-, two-, and three-body parts of the Hamiltonian. For example, for a Hartree-Fock (HF) reference state, E is the Hartree-Fock energy, and f is the Fock operator, which is diagonal in the eigenbasis of the HF one-body density matrix. The physical ground state of the system is not a single Slater determinant but some linear combination of $|\Phi\rangle$ and its elementary excitations, leading to an energy lower than the reference-state expectation value. In the IMSRG and other many-body methods, the task is to calculate the remaining correlation energy beyond the Hartree-Fock level to obtain the exact ground-state energy.

B. In-medium similarity renormalization group

The similarity renormalization group (SRG) [36–39] seeks to construct a continuous unitary transformation of the Hamiltonian in the flow parameter s,

$$H(s) = U(s) H U^\dagger(s) , \tag{9}$$

which can be obtained by solving the flow equation

$$\frac{dH(s)}{ds} = [\eta(s), H(s)] , \tag{10}$$

where the initial condition is $H(s = 0) = H$ and the choice of the anti-Hermitian generator $\eta(s)$ fixes the unitary transformation generated over the course of the SRG evolution.

When $H(s)$ and $\eta(s)$ are vacuum normal ordered, the "free-space" SRG evolution of potentials can be used to reduce couplings between low and high momenta for two- and three-nucleon potentials. These "softened" potentials exhibit improved many-body convergence. At the same time, the evolution induces many-body forces, a fact one can quickly verify by considering the commutator in second-quantized form. The treatment of many-body interactions in the free-space SRG approach is limited by the exponential cost of representing the A-body Hamiltonian in a Jacobi or single-particle basis, restricting this approach to the consistent evolution of two- and three-body forces [10, 40, 41].

In the IMSRG [14], $H(s)$ and $\eta(s)$ are normal ordered with respect to $|\Phi\rangle$, and the expression for the commutator is brought into normal order using Wick's theorem [42]. The in-medium normal ordering captures many of the effects of induced many-body interactions, which are always present in SRG evolutions, through lower-body interactions of the normal-ordered Hamiltonian. This is the feature that allows the IMSRG to succeed for the solution of the many-body Schrödinger equation for large systems where the SRG quickly becomes computationally intractable.

The generator $\eta(s)$ in SRG applications is typically chosen to decouple certain parts of the Hamiltonian over the course of the evolution. In the single-reference IMSRG, $\eta(s)$ is chosen to suppress couplings between the reference state and its elementary excitations [15], such that

$$\langle\Phi|H(s\to\infty)|\Phi^{a\cdots}_{i\cdots}\rangle = 0\,. \tag{11}$$

When this decoupling is achieved, the unitary transformation generated by the IMSRG is such that the matrix element $\langle\Phi|H(s\to\infty)|\Phi\rangle = E(s\to\infty)$ is the correlated energy of the state targeted by the reference state.

C. Truncation schemes

The IMSRG formalism is exact if one is able to keep track of all induced normal-ordered many-body contributions, as it is simply a unitary transformation on the many-body Hamiltonian that decouples the matrix element $\langle\Phi|H|\Phi\rangle$ from the remaining matrix elements. For practical calculations, the IMSRG solution must be restricted to include only the operators up to some fixed particle rank. The current standard truncation for nuclear structure applications is the IMSRG(2), where all operators are truncated at the normal-ordered two-body level:

$$H(s) = E(s) + f(s) + \Gamma(s)\,, \tag{12}$$

$$\eta(s) = \eta^{(1)}(s) + \eta^{(2)}(s)\,. \tag{13}$$

At this truncation, there are two approximations present. First, for Hamiltonians with three-body interactions, the residual normal-ordered three-body part of the Hamiltonian $W(s=0)$ is discarded, which is the so-called normal-ordered two-body (NO2B) approximation [43, 44]. Second, the commutator $[\eta^{(2)}(s), \Gamma(s)]$ has a normal-ordered three-body part, which is discarded in the IMSRG(2). Some attempts to approximately capture the effects of neglected induced three-body contributions in the IMSRG(2) have been explored [45], but a systematic understanding has not been formed.

The IMSRG(2) approximation has several desirable features as a many-body method. It scales polynomially [specifically like $O(N^6)$] in the size of the single-particle basis N. It is complete up to third order in MBPT, but it is also nonperturbative in that it resums pp/hh-ladder and ph-ring diagrams [15]. Additionally, it is size extensive, meaning that its error scales linearly in the size of the system. This puts the IMSRG(2) in the same category as many-body methods like CCSD [12] and ADC(3) [46], which are also nonperturbative and third-order complete but differ from the IMSRG(2) in what higher-order MBPT contributions the methods include.

III. IMSRG(3)

Extending the IMSRG to the normal-ordered three-body level yields the IMSRG(3) approximation. The Hamiltonian and the generator now each have a normal-ordered three-body part,

$$H(s) = E(s) + f(s) + \Gamma(s) + W(s)\,, \tag{14}$$

$$\eta(s) = \eta^{(1)}(s) + \eta^{(2)}(s) + \eta^{(3)}(s)\,, \tag{15}$$

and this makes it possible to include the initial residual three-body interactions exactly in the IMSRG(3) calculation.

A. Fundamental commutators

The IMSRG truncations are typically derived and implemented in terms of the fundamental commutators of two many-body operators. These fundamental commutators are the basic operations that need to be evaluated in any IMSRG calculation. For the commutator of a normal-ordered K-body operator $A^{(K)}$ and a normal-ordered L-body operator $B^{(L)}$, the resulting operator has different normal-ordered M-body parts $C^{(M)}$:

$$\left[A^{(K)}, B^{(L)}\right] = \sum_{M=|K-L|}^{K+L-1} C^{(M)}. \tag{16}$$

The fact that $M \le K+L-1$ for the commutator (as opposed to $M \le K+L$ for a simple product of normal-ordered operators) ensures that the many-body expansion is "connected," which means that the IMSRG at any truncation level is size extensive. We isolate the different M-body parts that arise from the commutator of a K-body operator and an L-body operator, using the following schematic notation in terms of their many-body ranks:

$$[K, L] \to M\,. \tag{17}$$

In the following, we provide the nonantisymmetrized expressions for the matrix elements of the fundamental commutators required by the IMSRG(3). For the two- and three-body parts, the matrix elements must be antisymmetrized by applying the appropriate two- and three-body antisymmetrizer. The expressions were derived using the automated normal-ordering tool DRUDGE [47], and, in cases where our expressions did not match those provided in Ref. [15], the results were verified by hand (see also the Appendices).

In the following sections, the section headings employ the schematic notation introduced above, where $[K, L] \to \circ$ is short for

$$\left[A^{(K)}, B^{(L)}\right] \to C\,. \tag{18}$$

1. $[1, 1] \to \circ$

$$C_{12} = \sum_p \left(A_{1p}B_{p2} - B_{1p}A_{p2}\right), \tag{19}$$

$$C^{(0)} = \sum_{pq} (n_p\bar{n}_q - \bar{n}_p n_q) A_{pq}B_{qp}\,, \tag{20}$$

with $\bar{n}_p \equiv 1 - n_p$ and the one-body matrix elements of the result C_{12}.

2. $[1,2] \to \circ$

$$C_{1234} = 2\sum_p \Big(A_{1p}B_{p234} - A_{p3}B_{12p4}\Big), \tag{21}$$

$$C_{12} = \sum_{pq}(n_p\bar{n}_q - \bar{n}_p n_q)A_{pq}B_{1q2p}\,. \tag{22}$$

3. $[2,2] \to \circ$

$$C_{123456} = 9\sum_p \Big(A_{3p45}B_{126p} - B_{3p45}A_{126p}\Big), \tag{23}$$

$$\begin{aligned} C_{1234} = {} & \frac{1}{2}\sum_{pq}(\bar{n}_p\bar{n}_q - n_p n_q) \\ & \times \Big(A_{12pq}B_{pq34} - B_{12pq}A_{pq34}\Big) \\ & - 4\sum_{pq}(n_p\bar{n}_q - \bar{n}_p n_q)A_{p23q}B_{1qp4}\,, \end{aligned} \tag{24}$$

$$\begin{aligned} C_{12} = {} & \frac{1}{2}\sum_{pqr}(\bar{n}_p\bar{n}_q n_r + n_p n_q\bar{n}_r) \\ & \times \Big(A_{1rpq}B_{pq2r} - B_{1rpq}A_{pq2r}\Big), \end{aligned} \tag{25}$$

$$C^{(0)} = \frac{1}{4}\sum_{pqrs}(n_p n_q\bar{n}_r\bar{n}_s - \bar{n}_p\bar{n}_q n_r n_s)A_{pqrs}B_{rspq}\,. \tag{26}$$

4. $[1,3] \to \circ$

$$C_{123456} = 3\sum_p \Big(A_{3p}B_{12p456} - A_{p6}B_{12345p}\Big), \tag{27}$$

$$C_{1234} = \sum_{pq}(n_p\bar{n}_q - \bar{n}_p n_q)A_{pq}B_{12q34p}\,. \tag{28}$$

5. $[2,3] \to \circ$

$$\begin{aligned} C_{123456} = {} & \frac{3}{2}\sum_{pq}(\bar{n}_p\bar{n}_q - n_p n_q) \\ & \times \Big(A_{12pq}B_{pq3456} - A_{pq45}B_{123pq6}\Big) \\ & + 9\sum_{pq}(\bar{n}_p n_q - n_p\bar{n}_q)A_{3pq6}B_{12q45p}\,, \end{aligned} \tag{29}$$

$$\begin{aligned} C_{1234} = {} & \sum_{pqr}(\bar{n}_p\bar{n}_q n_r + n_p n_q\bar{n}_r) \\ & \times \Big(A_{r1pq}B_{pq234r} - A_{pqr3}B_{12rpq4}\Big), \end{aligned} \tag{30}$$

$$C_{12} = \frac{1}{4}\sum_{pqrs}(n_p n_q\bar{n}_r\bar{n}_s - \bar{n}_p\bar{n}_q n_r n_s)A_{pqrs}B_{rs1pq2}\,. \tag{31}$$

6. $[3,3] \to \circ$

$$\begin{aligned} C_{123456} = {} & \frac{1}{6}\sum_{pqr}(n_p n_q n_r + \bar{n}_p\bar{n}_q\bar{n}_r) \\ & \times \Big(A_{123pqr}B_{pqr456} - B_{123pqr}A_{pqr456}\Big) \\ & + \frac{9}{2}\sum_{pqr}(\bar{n}_p\bar{n}_q n_r + n_p n_q\bar{n}_r) \\ & \times \Big(A_{pq345r}B_{12rpq6} - B_{pq345r}A_{12rpq6}\Big), \end{aligned} \tag{32}$$

$$\begin{aligned} C_{1234} = {} & \frac{1}{6}\sum_{pqrs}(\bar{n}_p\bar{n}_q\bar{n}_r n_s - n_p n_q n_r\bar{n}_s) \\ & \times \Big(A_{12spqr}B_{pqr34s} - B_{12spqr}A_{pqr34s}\Big) \\ & + \sum_{pqrs}(n_p n_q\bar{n}_r\bar{n}_s - \bar{n}_p\bar{n}_q n_r n_s)A_{pq1rs3}B_{rs2pq4}\,, \end{aligned} \tag{33}$$

$$\begin{aligned} C_{12} = {} & \frac{1}{12}\sum_{pqrst}(n_p n_q n_r\bar{n}_s\bar{n}_t + \bar{n}_p\bar{n}_q\bar{n}_r n_s n_t) \\ & \times \Big(A_{st1pqr}B_{pqrst2} - B_{st1pqr}A_{pqrst2}\Big), \end{aligned} \tag{34}$$

$$\begin{aligned} C^{(0)} = {} & \frac{1}{36}\sum_{pqrstu}(n_p n_q n_r\bar{n}_s\bar{n}_t\bar{n}_u - \bar{n}_p\bar{n}_q\bar{n}_r n_s n_t n_u) \\ & \times A_{pqrstu}B_{stupqr}\,. \end{aligned} \tag{35}$$

The computational cost of each commutator scales naively like $O(N^{K+L+M})$ in the size of the single-particle basis N. As a result, the cost of the full IMSRG(3) solution scales like the cost of the $[3,3] \to 3$ commutator, $O(N^9)$. The full IMSRG(3) flow equations for the matrix elements of the Hamiltonian are provided in Appendix A along with a list of the differences between the expressions we provide and those given in Ref. [15].

B. Generators

In the IMSRG(3), the extended many-body truncation introduces new matrix elements of the Hamiltonian that couple the reference state and its excitations, specifically W_{ijkabc} and W_{abcijk}, where i, j, and k are hole-state indices and a, b, and c are particle-state indices. Below we extend the standard generator definitions used in the single-reference IMSRG(2) [15] to the three-body case, seeking to suppress these matrix elements over the course of the evolution.

For the imaginary-time generator, we choose the matrix elements of the three-body part of the generator to be

$$\eta_{ijkabc} = \mathrm{sgn}(\Delta_{ijkabc})W_{ijkabc}\,, \tag{36a}$$

$$\eta_{abcijk} = \mathrm{sgn}(\Delta_{abcijk})W_{abcijk}\,, \tag{36b}$$

where we use the Møller-Plesset energy denominators

$$\Delta_{ijkabc} = f_{ii} + f_{jj} + f_{kk} - (f_{aa} + f_{bb} + f_{cc}) = -\Delta_{abcijk}\,. \tag{37}$$

Similarly, the matrix elements of the three-body White generator are chosen to be

$$\eta_{ijkabc} = \frac{W_{ijkabc}}{\Delta_{ijkabc}}\,, \tag{38a}$$

$$\eta_{abcijk} = \frac{W_{abcijk}}{\Delta_{abcijk}}\,, \tag{38b}$$

and the matrix elements of the three-body arctan generator are chosen to be

$$\eta_{ijkabc} = \frac{1}{2}\arctan\left(\frac{2W_{ijkabc}}{\Delta_{ijkabc}}\right), \tag{39a}$$

$$\eta_{abcijk} = \frac{1}{2}\arctan\left(\frac{2W_{abcijk}}{\Delta_{abcijk}}\right). \tag{39b}$$

C. Perturbative analysis

In Ref. [15], a perturbative analysis of the IMSRG is presented for the case where the NO2B approximation and an HF reference state are used. This analysis reveals the MBPT diagrammatic content of the many-body method, and we use it as a tool to understand the contributions of different commutators in the IMSRG(3). In the following we present the key ideas of the perturbative analysis and refer the reader interested in a more formal treatment to Ref. [15].

The connection from the IMSRG to MBPT is cleanly made when using the White generator, with the matrix elements

$$\eta_{ia} = \frac{f_{ia}}{\Delta_{ia}}\,, \tag{40a}$$

$$\eta_{ijab} = \frac{\Gamma_{ijab}}{\Delta_{ijab}}\,, \tag{40b}$$

$$\eta_{ijkabc} = \frac{W_{ijkaba}}{\Delta_{ijkabc}}\,, \tag{40c}$$

where Δ_{ia} and Δ_{ijab} are defined analogously to Eq. (37). Here and in the following i, j, and k are hole single-particle indices, and a, b, and c are particle single-particle indices. Using this generator, the zero-body part of the IMSRG flow equations (up to the three-body level) has three contributions from the $[1,1]\to 0$, $[2,2]\to 0$, and $[3,3]\to 0$ commutators,

$$\begin{aligned}\left(\frac{dE}{ds}\right)_{110} &= \sum_{ia}\left(\eta_{ia}(s)f_{ai}(s) - \eta_{ai}(s)f_{ia}(s)\right)\\ &= 2\sum_{ia}\eta_{ia}(s)f_{ai}(s) = 2\sum_{ia}\frac{f_{ia}(s)f_{ai}(s)}{\Delta_{ia}(s)}\,,\end{aligned} \tag{41}$$

$$\begin{aligned}\left(\frac{dE}{ds}\right)_{220} &= \frac{1}{2}\sum_{ijab}\eta_{ijab}(s)\Gamma_{abij}(s)\\ &= \frac{1}{2}\sum_{ijab}\frac{\Gamma_{ijab}(s)\Gamma_{abij}(s)}{\Delta_{ijab}(s)}\,,\end{aligned} \tag{42}$$

$$\begin{aligned}\left(\frac{dE}{ds}\right)_{330} &= \frac{1}{18}\sum_{ijkabc}\eta_{ijkabc}(s)W_{abcijk}(s)\\ &= \frac{1}{18}\sum_{ijkabc}\frac{W_{ijkabc}(s)W_{abcijk}(s)}{\Delta_{ijkabc}(s)}\,,\end{aligned} \tag{43}$$

which look remarkably similar to the second-order MBPT corrections to the energy. Indeed, if one approximates the hole-particle block matrix elements $f_{ia}(s)$, $\Gamma_{ijab}(s)$, and $W_{ijkabc}(s)$ by their basic suppression behavior due to the White generator [15],

$$f_{ia}(s) \approx f_{ia}(s=0)\exp(-s)\,, \tag{44a}$$

$$\Gamma_{ijab}(s) \approx \Gamma_{ijab}(s=0)\exp(-s)\,, \tag{44b}$$

$$W_{ijkabc}(s) \approx W_{ijkabc}(s=0)\exp(-s)\,, \tag{44c}$$

and one approximates the energy denominators by their initial values, then Eqs. (41)–(43) can be analytically integrated to get the results

$$E(s\to\infty)_{110} \approx \sum_{ia}\frac{f_{ia}(s=0)f_{ai}(s=0)}{\Delta_{ia}(s=0)}\,, \tag{45}$$

$$E(s\to\infty)_{220} \approx \frac{1}{4}\sum_{ijab}\frac{\Gamma_{ijab}(s=0)\Gamma_{abij}(s=0)}{\Delta_{ijab}(s=0)}\,, \tag{46}$$

$$E(s\to\infty)_{330} \approx \frac{1}{36}\sum_{ijkabc}\frac{W_{ijkabc}(s=0)W_{abcijk}(s=0)}{\Delta_{ijkabc}(s=0)}\,. \tag{47}$$

These are exactly the second-order MBPT corrections to the energy, and this shows that these corrections are absorbed into the IMSRG correlation energy, making the IMSRG at any many-body truncation second-order complete in MBPT (as long as the matrix elements are able to be captured initially in the many-body truncation).

Extending this analysis to higher orders in MBPT requires considering how the hole-particle matrix elements of f, Γ, and W change over the course of the IMSRG evolution beyond the basic suppression of their initial values. On a high level, this corresponds to the IMSRG evolution "dressing" the one-, two-, and three-body vertices with effective interaction contributions that generate higher-order MBPT diagrams.

To make this analysis systematic, we focus on the case where we use an HF reference state and work in the NO2B approximation, where the initial off-diagonal matrix elements of f and all the initial matrix elements of W are 0. Working with a Møller-Plesset MBPT partitioning of the initial Hamiltonian,

$$H = f + g\,\Gamma\,, \tag{48}$$

we have the following power-counting scheme:

$$f_{pp} = O(g^0)\,, \tag{49}$$

$$\Gamma_{pqrs} = O(g^1)\,, \tag{50}$$

that is, the diagonal one-body matrix elements are $O(g^0)$ and the two-body matrix elements are $O(g^1)$. In this case, the hole-particle block of f is induced by the $[2,2]\to 1$ commutator (the $[1,2]\to 1$ commutator initially does not induce hole-particle contributions because f_{ia} and thus $\eta^{(1)}$ are 0), and the matrix elements of W are induced by the $[2,2]\to 3$ commutator. This means

$$f_{ia} = O(g^2)\,, \tag{51}$$

$$W_{pqrstu} = O(g^2)\,, \tag{52}$$

Commutator	Cost	Perturbative order
$[1,1] \to 0$	$O(N^2)$	g^4
$[1,1] \to 1$	$O(N^3)$	g^4
$[1,2] \to 1$	$O(N^4)$	g^5
$[1,2] \to 2$	$O(N^5)$	g^2
$[2,2] \to 0$	$O(N^4)$	g^2
$[2,2] \to 1$	$O(N^5)$	g^4
$[2,2] \to 2$	$O(N^6)$	g^3
$[2,2] \to 3$	$O(N^7)$	g^4
$[1,3] \to 2$	$O(N^6)$	g^5
$[1,3] \to 3$	$O(N^7)$	g^4
$[2,3] \to 1$	$O(N^6)$	g^5
$[2,3] \to 2$	$O(N^7)$	g^4
$[2,3] \to 3$	$O(N^8)$	g^5
$[3,3] \to 0$	$O(N^6)$	g^4
$[3,3] \to 1$	$O(N^7)$	g^6
$[3,3] \to 2$	$O(N^8)$	g^5
$[3,3] \to 3$	$O(N^9)$	g^6

TABLE I. The lowest-order perturbative contribution to the energy provided by each of the fundamental commutators along with their computational cost.

and, as a result, their contributions to the energy are both $O(g^4)$. [1]

Thus, the contribution of any induced two-body parts to E is suppressed by $O(g^1)$, and the contributions of induced one- and three-body parts to E are suppressed by $O(g^2)$. This allows one to quickly perturbatively estimate the importance of different fundamental commutators, provided in Table I.

It is worth noting that the $[1,1] \to 1$, $[1,2] \to 2$, and $[1,3] \to 3$ commutators have higher perturbative importance than their $[1,2] \to 1$, $[2,2] \to 2$, and $[2,3] \to 3$ counterparts, a consequence of the fact that they are sensitive to the diagonal part of f, which is $O(g^0)$. The former $[1,B] \to B$ commutators are responsible for the suppression of the B-body hole-particle blocks of the Hamiltonian and play a central role in the behavior of the IMSRG evolution. This is intuitively similar to the central role the kinetic energy plays in the free-space SRG.

A key result of the analysis in Ref. [15] is that the IMSRG(2) is complete up to third order in MBPT and contains many fourth-order diagrams as well. At the NO2B level, the IMSRG(3) accounts for the induced three-body effects, which are what is missing for the complete inclusion of fourth-order diagrams in the IMSRG(2), making the IMSRG(3) fourth-order complete (at the NO2B level) [15].

[1] This is true both for the direct flow into the energy via, for example, the $[3,3] \to 0$ commutator ($g^2 \times g^2$) and for the indirect case via an induced two-body part from, for example, the $[2,3] \to 2$ commutator followed by the flow into the energy through the $[2,2] \to 0$ commutator ($g^1 \times g^2 \times g^1$).

D. Approximation schemes

Due to the high computational cost of full IMSRG(3) calculations, finding a way to approximate the IMSRG(3) truncation would pave the way to large model-space IMSRG calculations that approximately include the effects of three-body operators. In the following, we present approximation schemes by including in each scheme selected IMSRG(3) fundamental commutators on top of the IMSRG(2).

The first major truncation beyond IMSRG(2) we use includes the minimum commutators necessary to make the truncation fourth-order complete in MBPT. These are the $[2,2] \to 3$, $[2,3] \to 2$, $[1,3] \to 3$, and $[3,3] \to 0$ commutators. We refer to this truncation as the IMSRG(3)-MP4 approximation. The IMSRG(3)-MP4 is most similar to iterated coupled-cluster methods like CCSDT-1 [12, 23, 48], as both methods are fourth-order complete. However, CCSDT-1 scales like $O(A^3N^4)$ [naively $O(N^7)$, but A is up to an order of magnitude smaller than N in converged calculations], while the IMSRG(3)-MP4 scales like $O(N^7)$.

We note that in our studies we found that the $[2,2] \to 3$, $[2,3] \to 2$, and $[1,3] \to 3$ commutators are required at the NO2B level for an approximate IMSRG(3) truncation to include some three-body effects and also be numerically stable. Without the $[2,2] \to 3$ and $[2,3] \to 2$ commutators, the zero- through two-body parts and the three-body part are decoupled, and the results remain identical to the IMSRG(2) results. Without the $[1,3] \to 3$ commutator, the induced three-body part is not properly suppressed over the course of the evolution, and the correlation energy does not seem to converge.

Beyond the IMSRG(3)-MP4 truncation, we consider two approaches to including further commutators. The first is inclusion based on computational cost, including first the cheapest of the remaining commutators before including the more expensive commutators [49]. The rationale here is that by using this approach one can include as much "physics" as possible while increasing the computational cost incrementally, hopefully leading to a fairly faithful reproduction of the full IMSRG(3) results. The second approach is based on the perturbative analysis discussed in Sec. III C, where remaining commutators are included in the order of their perturbative importance. This physically motivated approach attempts to capture as best as possible the available physics in a consistent manner before including "higher-order" effects. One would hope to see that these higher-order effects generate only small changes in energies and in practical calculations some "complete" lower-order approximation could be used.

Following the first approach, including the $[2,3] \to 1$, $[1,3] \to 2$, and $[3,3] \to 1$ commutators on top of the IMSRG(3)-MP4 approximation yields a truncation that includes all IMSRG(3) commutators that cost $O(N^7)$ or less. We refer to this truncation as the IMSRG(3)-N^7 truncation. The inclusion of the $[2,3] \to 3$ and $[3,3] \to 2$ commutators on top of this truncation yields the IMSRG(3)-N^8 truncation, which includes all commutators that cost $O(N^8)$ or less. This truncation differs from the full IMSRG(3) only by the missing $[3,3] \to 3$ commutator.

Commutator	Cost	Included in …				
		IMSRG(3)-MP4	IMSRG(3)-N^7	IMSRG(3)-N^8	IMSRG(3)-g^5	IMSRG(3)
$[2,2] \to 3$	$O(N^7)$	✓	✓	✓	✓	✓
$[2,3] \to 2$	$O(N^7)$	✓	✓	✓	✓	✓
$[1,3] \to 3$	$O(N^7)$	✓	✓	✓	✓	✓
$[3,3] \to 0$	$O(N^6)$	✓	✓	✓	✓	✓
$[2,3] \to 1$	$O(N^6)$		✓	✓	✓	✓
$[1,3] \to 2$	$O(N^6)$		✓	✓	✓	✓
$[3,3] \to 1$	$O(N^7)$		✓	✓		✓
$[2,3] \to 3$	$O(N^8)$			✓	✓	✓
$[3,3] \to 2$	$O(N^8)$			✓	✓	✓
$[3,3] \to 3$	$O(N^9)$					✓

TABLE II. The computational cost of the IMSRG(3) fundamental commutators and whether they are included in various approximate and full IMSRG(3) truncation schemes.

Following the second approach, we note that the IMSRG(3)-MP4 truncation already follows this approach, including all of the IMSRG(3) commutators that are $O(g^4)$ or less, with the exception of the $[1,2] \to 1$ commutator, which is $O(g^5)$ and is included in the IMSRG(2) truncation. The next truncation we present includes the remaining $O(g^5)$ commutators, the $[2,3] \to 1$, $[1,3] \to 2$, $[2,3] \to 3$, and $[3,3] \to 2$ commutators, on top of the IMSRG(3)-MP4 truncation. We refer to this truncation as the IMSRG(3)-g^5 truncation. This truncation includes two commutators that cost $O(N^8)$, making that the cost of the truncation. The two remaining commutators are $O(g^6)$, so this is the only complete perturbatively guided truncation between the IMSRG(3)-MP4 and full IMSRG(3) truncations.

The inclusion of specific commutators in each of the approximate IMSRG(3) truncation schemes discussed above is presented in Table II.

IV. APPLICATIONS

In this section, we investigate the IMSRG(3) truncation and the approximate truncations discussed in Sec. III D when applied to the closed-shell ^{4}He and ^{16}O using different nuclear Hamiltonians.

A. Hamiltonians and basis sets

For most of our calculations, we focus on two sets of chiral Hamiltonians, one using the N^{3}LO nucleon-nucleon (NN) potential from Ref. [50] SRG-evolved to a resolution scale $\lambda = 1.8\,\mathrm{fm}^{-1}$, which we refer to as the "EM 1.8" Hamiltonian, and one using the "EM 1.8/2.0" potential from Ref. [6] with both NN and three-nucleon ($3N$) interactions. For the treatment of the three-body part of the NN+$3N$ Hamiltonian when using the EM 1.8/2.0 potential, we use the NO2B approximation [43, 44].

In Sec. IV E, we explore how the trends seen for the soft EM 1.8 and EM 1.8/2.0 Hamiltonians are affected by the choice of harder Hamiltonians. We use three sets of NN-only Hamiltonians. One uses the N^{3}LO NN potential from Ref. [50] (with no SRG evolution applied), which we refer to as the "EM 500" Hamiltonian based on its regulator cutoff at $\Lambda = 500$ MeV. The other two use the N^{3}LO NN potential from Ref. [8] with $\Lambda = 450$ MeV (referred to as the "EMN 450" Hamiltonian) and $\Lambda = 500$ MeV (referred to as "EMN 500").

In addition, we use reference states constructed from different single-particle basis sets. Our single-particle basis is characterized by the maximum principal quantum number $e_{\max} = (2n + l)_{\max}$, with the radial quantum number n and the orbital angular momentum l. In the simplest case, we solve the spherically restricted HF equations to obtain a variationally optimized HF solution. Where an HF reference state is used, the solution of the HF equations and the solution of the IMSRG both take place in an $e_{\max} = 2$ model space. The HF calculations were performed using the solver from Ref. [51].

As an alternative, we use so-called natural orbitals (NAT), which are defined as the eigenstates of the one-body density matrix. Following the prescription detailed in Ref. [52], the one-body density matrix is expanded up to second order in perturbation theory, which incorporates dynamic particle-hole correlation effects in the construction of the single-particle basis, leading to improved convergence properties and reduced sensitivity to the underlying basis frequency [53, 54]. We follow the strategy of Ref. [54], where the one-body density matrix is constructed in a large model space with $e_{\max}^{\mathrm{NAT}}$. Following the construction of the basis and the transformation of the Hamiltonian matrix elements, the basis and operators are truncated to a model space with a smaller $e_{\max}$, which is used for the IMSRG solution.

When using NN-only Hamiltonians, the construction of the NAT basis takes place in an $e_{\max}^{\mathrm{NAT}} = 14$ model space. The basis and Hamiltonian are truncated to an $e_{\max} = 2$ model space for the following IMSRG calculation. When using the EM 1.8/2.0 NN+$3N$ Hamiltonian, the construction of the NAT basis takes place in an $e_{\max}^{\mathrm{NAT}} = 14$ model space with an additional $E_{3,\max} = 16 \geq e_1 + e_2 + e_3$ truncation placed on the three-body

matrix elements. Again, the basis and Hamiltonian are truncated to an $e_{\max} = 2$ model space for the following IMSRG calculation.

The IMSRG calculations presented here all use the imaginary-time generator and solve the IMSRG by directly integrating the flow equations (as opposed to using the Magnus-expansion approach [55]). For the single-reference IMSRG(2), it was found that the choice of the generator (between the imaginary-time, White, and arctan generators) only has a very small effect on the result of the IMSRG solution [15]. We also experimented with generator choice in the IMSRG(3) case and found that choosing a different generator changed the results obtained for each truncation scheme by less than 1 keV, an effect much smaller than the effects we discuss in the following sections. It seems that the insensitivity to generator choice in the IMSRG(2) extends also to the IMSRG(3).

B. Helium-4

In this section, we consider how the IMSRG solution for the ground-state energy of ^{4}He changes for different truncation schemes ranging from the IMSRG(2) to the full IMSRG(3) approximation. We focus our discussion on the major truncations discussed in Sec. III D and presented succinctly in Table II. In the figures like Fig. 1, these truncations are visually indicated by the thicker bars. We also introduce minor truncations, which are defined as having one additional commutator included relative to some previous truncation scheme. For example, one minor truncation scheme we consider is the IMSRG(3)-N^7 + $[2,3] \rightarrow 3$ truncation, which has all $O(N^7)$ commutators and the $[2,3] \rightarrow 3$ commutator, which is $O(N^8)$. The inclusion of the $[3,3] \rightarrow 2$ commutator on top of this truncation yields another major truncation, the IMSRG(3)-N^8 truncation. These minor truncations are visually indicated by thinner bars.

We first focus on the case where we use the EM 1.8 *NN*-only Hamiltonian. For the *NN*-only case, we use an underlying oscillator frequency of $\hbar\Omega = 28$ MeV, which was determined by choosing the frequency at which the ground-state energy that resulted from IMSRG(2) calculations using an HF reference state was minimal. For comparison, we provide exact results from the full configuration interaction (FCI) diagonalization of the $e_{\max} = 2$ Hamiltonian. In the absence of a many-body truncation, this would be the exact result the IMSRG would be able to obtain, and comparing against this result for different approximations allows us to gain insight into the effect of the many-body truncations at play.

In Fig. 1, we show the ground-state energies for ^{4}He obtained using different IMSRG truncation schemes using the EM 1.8 *NN*-only Hamiltonian and an HF reference state. In both panels, we start from the IMSRG(2) truncation and add commutators until we reach the IMSRG(3) truncation on the right.

In the left panel of Fig. 1, we follow the computational approach to organizing the IMSRG(3) fundamental commutators. At the IMSRG(2)-truncation level, the ground-state energy only differs from the FCI result by 9 keV. The first truncation we consider beyond the IMSRG(2) is always the IMSRG(3)-MP4 truncation, which in all systems we investigated delivered a sizable repulsive correction to the energy. This is consistent with our understanding of the diagrammatic content of the IMSRG(2) and the nature of the missing fourth-order MBPT energy corrections. The inclusion of fundamental commutators up to the IMSRG(3)-N^7 truncation brings the correlated energy back down towards the FCI result. The next two commutators that are included in the IMSRG(3)-N^8 truncation provide significant contributions that partially cancel. The size of their individual contributions can be understood by the fact that they are both fifth-order [$O(g^5)$] in our perturbative counting [to be compared with the $O(g^6)$ contribution of $[3,3] \rightarrow 1$, which is the final commutator that contributes to the IMSRG(3)-N^7]. The contribution of the $[3,3] \rightarrow 3$ commutator to arrive at the full IMSRG(3) truncation is small, and the final IMSRG(3) ground-state energy differs from the FCI result by 8 keV.

In the right panel, we show the same information for the case where the perturbative ordering of fundamental commutators is used. We see that the $O(g^5)$ commutators added from the IMSRG(3)-MP4 truncation to the IMSRG(3)-g^5 truncation deliver contributions to the energy that are generally smaller than the fourth-order shift between IMSRG(2) and IMSRG(3)-MP4 truncations and generally larger than the sixth-order shifts between the IMSRG(3)-g^5 and the IMSRG(3) truncations, which is consistent with the perturbative counting.

When discussing the contributions of commutators, it is worth noting that the contribution of an added commutator to the energy also depends on which other commutators are also included in that truncation. In this context, the one-by-one inclusion of fundamental commutators formally does not commute. In practice, however, we see that the size of the contribution of a specific commutator is not strongly sensitive to the order in which it is included relative to other commutators. One can see this behavior when comparing the two panels of Fig. 1. Of course, substantial rearrangement of the commutators (in particular, changing the order of two commutators that give large contributions to the energy) can change this picture. Our discussion, however, is built around the major truncation schemes discussed in Sec. III D, restricting the freedom we have to move commutators around in between. As far as we have seen in our explorations, the quasiadditive nature of the inclusion of commutators and their energy contributions seems to qualitatively hold within these restrictions.

In Fig. 2, we present results for ^{4}He when using the EM 1.8 *NN*-only Hamiltonian and a NAT reference state. The same oscillator frequency is used as for the *NN*-only HF case ($\hbar\Omega = 28$ MeV). The IMSRG(2) error to the FCI result is in this case 27 keV. In the left panel, following the repulsive IMSRG(3)-MP4 corrections to the energy, we see that the commutators added to give the IMSRG(3)-N^7 give additional small repulsive shifts to the energy. The $O(N^8)$ commutators give slightly larger attractive contributions, and the $[3,3] \rightarrow 3$ commutator again delivers a very small contribution. The final IMSRG(3) energy differs from the FCI result by 9 keV. This is a considerable improvement over the IMSRG(2) result, al-

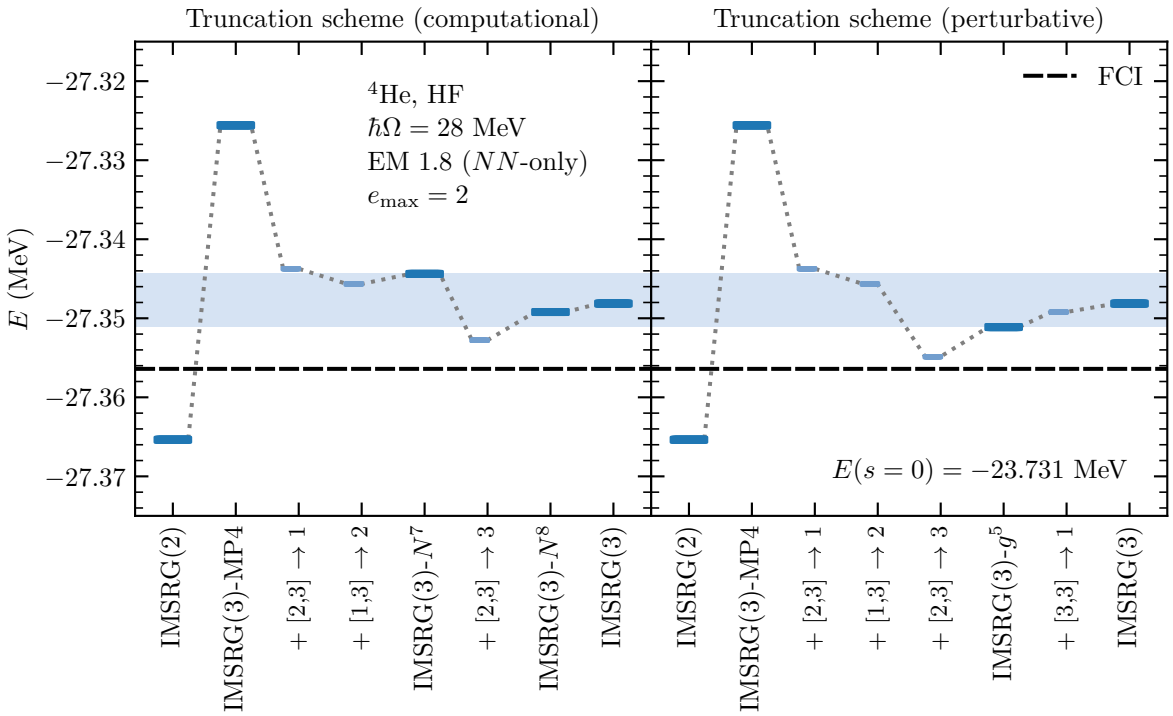

FIG. 1. Ground-state energies of ^{4}He obtained in various truncation schemes using the EM 1.8 NN-only Hamiltonian and an HF reference state following the computational (left panel) and perturbative (right panel) truncation ordering for the fundamental commutators. Thicker, darker bars correspond to the major truncations summarized in Table II. Thinner, lighter bars correspond to intermediate truncations where a single fundamental commutator has been added relative to the truncation scheme to the left. The dashed line indicates the $e_{\max} = 2$ FCI result obtained for this Hamiltonian. The blue band indicates the range spanned by the results obtained from the IMSRG(3)-N^7 and IMSRG(3)-g^5 truncations. The starting HF energy is provided in the bottom right corner.

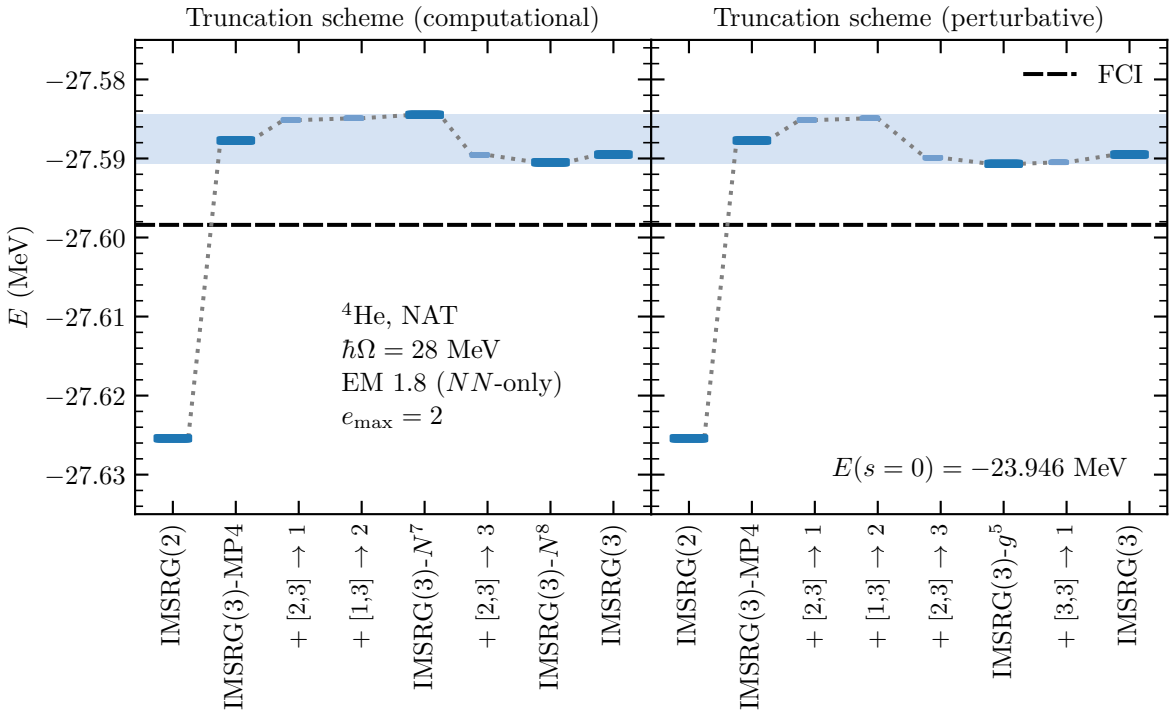

FIG. 2. Same as Fig. 1 but using a NAT reference state.

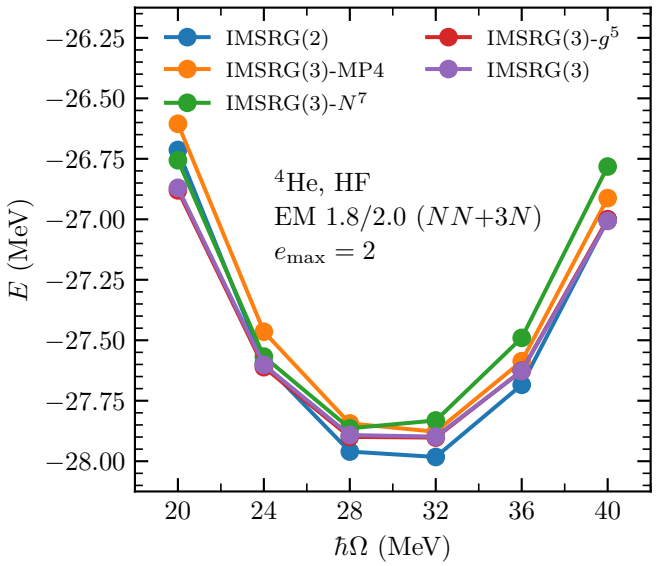

FIG. 3. Ground-state energies of ^{4}He using the EM 1.8/2.0 Hamiltonian and an HF reference state obtained in several IMSRG truncation schemes at a broad range of frequencies.

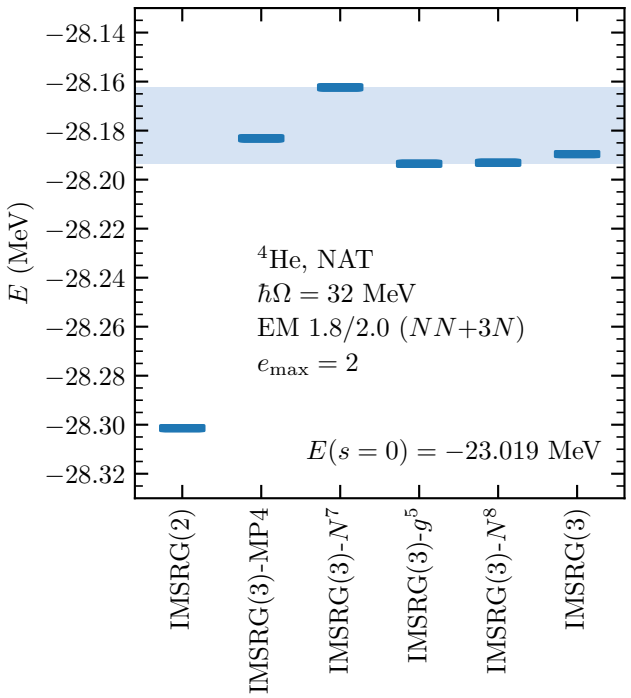

FIG. 4. Ground-state energies of ^{4}He obtained in various truncation schemes using the EM 1.8/2.0 Hamiltonian and a NAT reference state. The blue band indicates the range spanned by the results obtained from the IMSRG(3)-N^7 and IMSRG(3)-g^5 truncations. The starting energy of the NAT reference state is provided in the bottom right corner.

though all of the results discussed here are quite good (sub-1% error) when compared to the total ground-state energy or the correlation energy.

In the right panel, we see that the general size of energy contributions follows the perturbative counting. The size of all contributions beyond the IMSRG(3)-MP4 truncation is substantially smaller than in the HF case discussed previously (note that the relative scale on the energy in the graph is identical in Figs. 1 and 2). In particular, because the sixth-order commutator contributions are so small, the IMSRG(3)-g^5 approximates the full IMSRG(3) extremely well.

Now we switch our focus to the case where we use the EM 1.8/2.0 NN+3N Hamiltonian. We investigated the oscillator frequency sensitivity of the IMSRG(3) truncations in ^{4}He using an HF reference state. This system exhibits substantial frequency dependence because NN+3N Hamiltonians tend to give greater frequency dependence than their NN-only counterparts and the HF basis depends more strongly on the frequency than the NAT basis. This is because the NAT basis seeks to reduce frequency dependence by construction.

In Fig. 3, we show the ground-state energy obtained using several IMSRG truncations ranging from the IMSRG(2) to the IMSRG(3) for a broad range of oscillator frequencies. Generally, we find that the results for the different truncations remain quite close together (within a spread of 300 keV) even as the energy varies over a range of 1.5 MeV. This suggests that the variance in the energy is entirely due to harsh infrared and ultraviolet cutoffs imposed by the $e_{\max} = 2$ model space and not due to the many-body truncations, which would be improved by the IMSRG(3). It is of course possible that in calculations with larger model spaces one might see systematic differences in the frequency dependence of the energy resulting from different IMSRG truncations.

A couple systematic trends can be identified in Fig. 3. First, the IMSRG(3)-MP4 provides a repulsive contribution on top of the IMSRG(2) at all frequencies. Second, the IMSRG(3)-g^5 and IMSRG(3) lines lie basically on top of each other, indicating that the IMSRG(3)-g^5 reliably approximates the IMSRG(3). The same cannot be said for the IMSRG(3)-N^7. Finally, the IMSRG(3) results always lie below the IMSRG(3)-MP4 results.

In Fig. 4, we present the ^{4}He ground-state energies obtained in various IMSRG truncation schemes using the EM 1.8/2.0 Hamiltonian and a NAT reference state. The oscillator frequency of $\hbar\Omega = 32$ MeV was determined by choosing the frequency at which the HF IMSRG(2) energy result was minimal for this Hamiltonian (see Fig. 3). Overall, the corrections offered by approximate IMSRG(3) truncations are larger in magnitude than in the NN-only case, with the IMSRG(2) and IMSRG(3) results differing by 112 keV (compare with the difference of 36 keV in the NN-only case). We see similar trends as in the NN-only case, with a large repulsive correction from the IMSRG(3)-MP4 truncation and a smaller repulsive correction from the IMSRG(3)-N^7. The $O(N^8)$ fifth-order commutators provide attractive corrections, and the final IMSRG(3) result lands between the IMSRG(3)-N^7 and IMSRG(3)-g^5 results, as indicated by the blue band.

C. Oxygen-16

In this section, we consider the IMSRG solution for the ground-state energy of ^{16}O. We first focus on the case where we use the EM 1.8 *NN*-only Hamiltonian. In this case, we use an oscillator frequency of $\hbar\Omega = 24$ MeV. For *NN*-only results, we provide for comparison extrapolated FCI results. These results were obtained from a series of CI calculations with increasing $N_{\max}$ (the model space truncation for the approach) from 0 to 8 using the KSHELL code [56]. The results from $N_{\max} = 2$ to 8 were then fit to an exponential function to obtain the $N_{\max} \to \infty$ extrapolated value [57]. The uncertainty in the extrapolation was assessed by leaving out one of the $N_{\max} = 2, 4, 6$ points and fitting the exponential to the remaining three points (the highest-quality $N_{\max} = 8$ point was always included). The largest deviation from the full fit value and the subsampled fit values is taken to be the uncertainty.

In Fig. 5, we show the ground-state energies of ^{16}O as obtained from different truncation schemes when using an HF reference state. The IMSRG(2) result differs from the exact result by about 180 keV, which corresponds to an error of 1.8% in the correlation energy. The IMSRG(3)-MP4 approximation provides a large, repulsive correction to the IMSRG(2) result. In the left panel, we see that the $[2,3] \to 1$ commutator included in the IMSRG(3)-N^7 truncation provides a small, but significant attractive correction and the $[2,3] \to 3$ commutator included in the IMSRG(3)-N^8 delivers most of the remaining attraction needed to produce the IMSRG(3) result. The final IMSRG(3) result differs from the extrapolated FCI result by only 32 keV, which corresponds to an error of about 0.3% in the correlation energy. In the right panel, we see that the perturbative counting of commutators continues to be predictive, with the smallest contributions belonging to the sixth-order commutators. As a result, the IMSRG(3)-g^5 result lies quite close to the IMSRG(3) result.

In Fig. 6, we switch to a NAT reference state, still considering ^{16}O using the EM 1.8 *NN*-only Hamiltonian. The difference between the IMSRG(2) result and the exact result is only 16 keV, making the IMSRG(2) result in this case remarkably good. The correction provided by the IMSRG(3)-MP4 truncation is still repulsive, but considerably smaller than in the HF case. In the left panel, we see that again the $[2,3] \to 1$ and $[2,3] \to 3$ commutators deliver the main contributions to corrections provided by the IMSRG(3)-N^7 and IMSRG(3)-N^8 truncations, respectively. The final IMSRG(3) result differs from the extrapolated FCI result by 28 keV, quite similar to the difference in the HF case. The right panel shows that convergence to the IMSRG(3) result in the perturbative counting approach is systematic in this case as well.

Switching to the EM 1.8/2.0 Hamiltonian, we consider in Fig. 7 the IMSRG solution for various truncations for ^{16}O using a NAT reference state, where the underlying oscillator frequency is $\hbar\Omega = 20$ MeV. In this case, the IMSRG(3)-MP4 truncation result is about 270 keV more repulsive than the IMSRG(2) result, and the IMSRG(3)-N^7 provides only small corrections to the IMSRG(3)-MP4 result. These results differ substantially from those obtained from the remaining truncation schemes, which contain all the $O(N^8)$ fifth-order commutators. Of the systems we studied, this is the system with the largest contribution by these commutators, making the IMSRG(3)-g^5, for example, a substantial improvement over the IMSRG(3)-N^7 due to its inclusion of these higher-cost fifth-order commutators that are neglected in the IMSRG(3)-N^7. We see that again the large band resulting from the IMSRG(3)-N^7 and IMSRG(3)-g^5 results includes the IMSRG(3) result.

D. Analysis of truncation performance

Next, we consider the relative performance of the different IMSRG truncations over all systems considered. These trends are summarized in Fig. 8. In this figure, we compare the correlation energy, defined as

$$E_{\text{corr}} = E(s \to \infty) - E(s = 0)\,, \tag{53}$$

for the IMSRG(2) and approximate IMSRG(3) truncations relative to the IMSRG(3) correlation energy. The vertical line at $x = 1.0$ indicates the IMSRG(3) correlation energy. In the previous sections, we saw that in most cases the IMSRG(3) energies were closer to the exact results obtained via FCI and extrapolated FCI calculations (with the exception of the ^{16}O case with the EM 1.8 *NN*-only Hamiltonian and the NAT reference state). This intuitively matches the expected behavior of the many-body expansion, where including higher many-body ranks in the many-body expansion allows the truncated methods to systematically approach the exact result. In this figure and the following discussion, we frame things relative to the IMSRG(3) results, as the IMSRG(3) truncation is the "most complete" IMSRG result we have available.

Considering the performance of the IMSRG(2) relative to the IMSRG(3), we see that the difference in the correlation energy is about 1–2% for most systems. This also makes it clear how unusually good the IMSRG(2) results are in the exceptional ^{16}O *NN*-only NAT case, where the difference in the IMSRG(2) and IMSRG(3) results is closer to 0.1%. We also see that the IMSRG(2) results are systematically overbound relative to the IMSRG(3) results.

Turning our attention to the IMSRG(3)-MP4 truncation, we find that these results differ from the IMSRG(3) results by up to 1%. The results are also all less bound than the IMSRG(3) results, making the IMSRG(2) and IMSRG(3)-MP4 results lower and upper bounds on the IMSRG(3) result. Considering that the IMSRG(3)-MP4 is the least computationally expensive approximate IMSRG(3) truncation we considered, this provides a relatively cheap way to set a weak bound on where the IMSRG(3) result lands. In the case where the many-body expansion converges systematically, this bound should also encompass the effects of higher orders in the many-body expansion.

Turning our attention to the next two truncations, the IMSRG(3)-N^7 and IMSRG(3)-g^5 truncations, we find that the IMSRG(3)-N^7 results are generally less bound than the IMSRG(3) results by about 0.5% (1% in one case) and the IMSRG(3)-g^5 results are generally more bound by about 0.1%. The gray bands in Fig. 8 show the range of energies

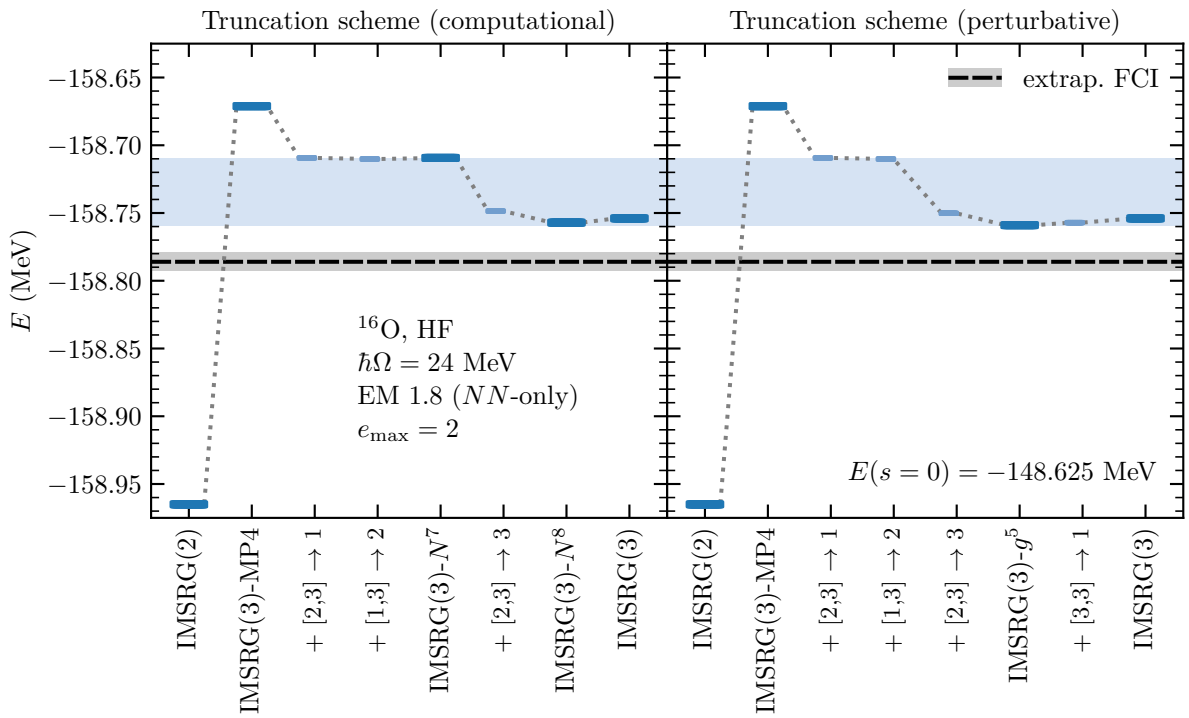

FIG. 5. Ground-state energies of ^{16}O obtained in various truncation schemes using the EM 1.8 NN-only Hamiltonian and an HF reference state following the computational (left panel) and perturbative (right panel) truncation ordering for the fundamental commutators. Thicker, darker bars correspond to the major truncations summarized in Table II. Thinner, lighter bars correspond to intermediate truncations where a single fundamental commutator has been added relative to the truncation scheme to the left. The dashed line indicates the $e_{\max} = 2$ extrapolated FCI result obtained for this Hamiltonian (see main text for details). The blue band indicates the range spanned by the results obtained from the IMSRG(3)-N^7 and IMSRG(3)-g^5 truncations. The starting HF energy is provided in the bottom right corner.

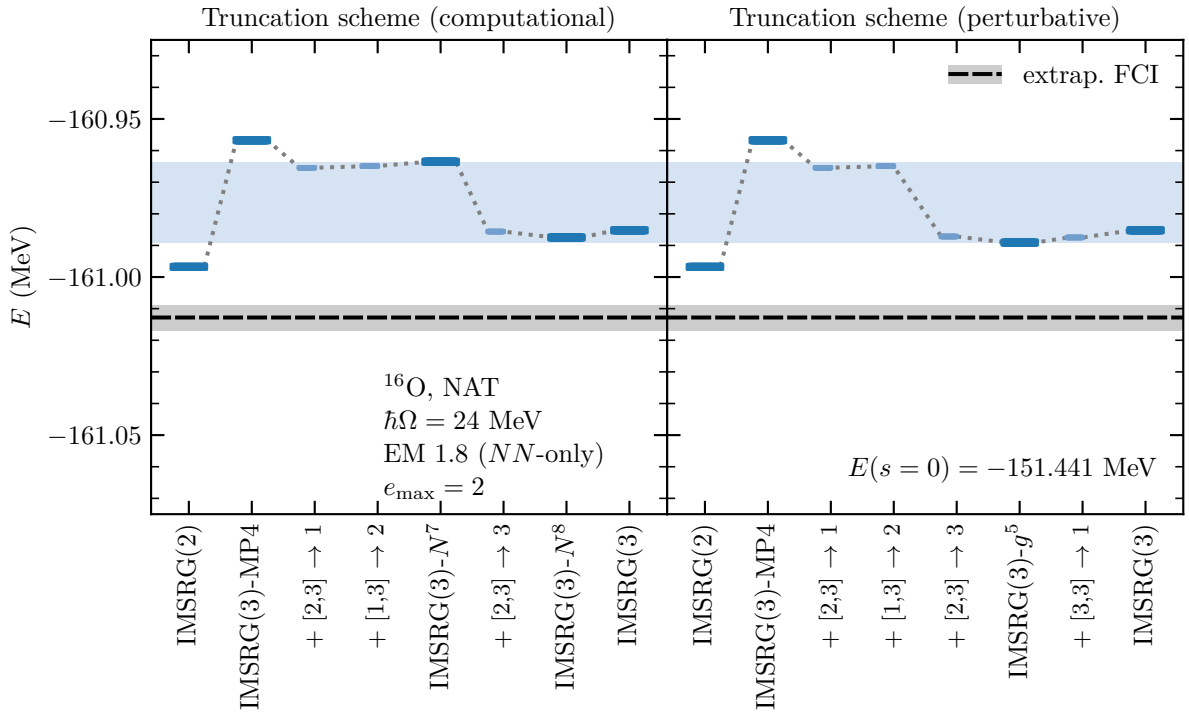

FIG. 6. Same as Fig. 5 but using a NAT reference state.

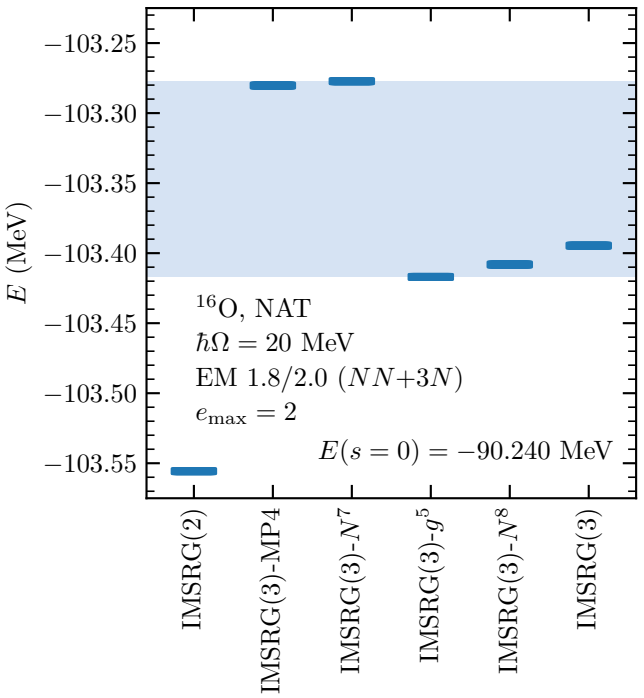

FIG. 7. Ground-state energies of ^{16}O obtained in various truncation schemes using the EM 1.8/2.0 Hamiltonian and a NAT reference state. The blue band indicates the range spanned by the results obtained from the IMSRG(3)-N^7 and IMSRG(3)-g^5 truncations. The starting energy of the NAT reference state is provided in the bottom right corner.

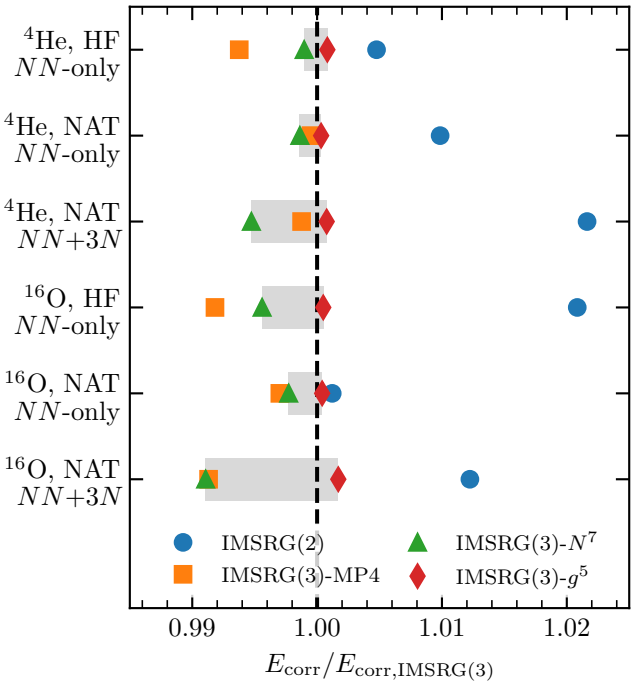

FIG. 8. Ratios of correlation energies obtained in IMSRG(2) and approximate IMSRG(3) calculations relative to the IMSRG(3) correlation energies for different systems discussed in Secs. IV B and IV C. The gray band indicates the range spanned by the IMSRG(3)-N^7 and IMSRG(3)-g^5 results.

bounded by the results from these two truncations, where we see that these bands always contain the IMSRG(3) results. The IMSRG(3)-N^7 is of comparable expense and quality to the IMSRG(3)-MP4 truncation. However, the IMSRG(3)-g^5 is considerably more expensive and nearly as expensive as the full IMSRG(3). This means that even once large-scale IMSRG(3)-MP4 and IMSRG(3)-N^7 are possible IMSRG(3)-g^5 calculations may still be out of reach. Still, if both IMSRG(3)-N^7 and IMSRG(3)-g^5 calculations are possible, then these can be used to provide a robust bound on what the IMSRG(3) results could be.

E. Performance for harder Hamiltonians

In Fig. 9, we show the error to the exact FCI ground-state energy of ^{4}He for the harder NN-only Hamiltonians for calculations using major and minor truncations schemes going from the IMSRG(2) approximation to the IMSRG(3) approximation. The correlation energies for these Hamiltonians are about 8 to 10 MeV, approximately double that of the EM 1.8 and EM 1.8/2.0 Hamiltonians in ^{4}He. We also note that the EM 500 Hamiltonian gives an unbound HF solution with a positive HF energy.

We see that for all three Hamiltonians the IMSRG(2) overbinds the system substantially relative to the exact result. These errors of about 350 to 500 keV correspond to errors of 3.5–5% in the correlation energy. The repulsive corrections from the IMSRG(3)-MP4 shift the obtained energies closer to the exact results. Going from the IMSRG(3)-MP4 truncation to the IMSRG(3)-N^7 and IMSRG(3)-g^5 truncations brings the IMSRG results within 100 keV of the exact results, a sub-1% error in the correlation energy. The higher-cost and higher-order corrections bring relatively small corrections, and the final IMSRG(3) results remain within 100 keV of exact energies for all three Hamiltonians. In Fig. 10, we show the results for ^{16}O. The approximate IMSRG(3) truncations systematically improve over the IMSRG(2), and the final IMSRG(3) results differ from the exact results by just over 100 keV, which is an error of about 0.5% in the correlation energy for both Hamiltonians. For the EM 500 Hamiltonian in the $e_{\max} = 2$ model space, the IMSRG(2) calculation of ^{16}O does not converge. The IMSRG(3) improves on this by delivering converged results that differ from exact results by about 3%, stabilizing the solution of IMSRG flow equations.

We see that the IMSRG(3) offers substantial, systematic improvements over the IMSRG(2). These improvements are largely already present in approximate IMSRG(3) truncations with lower computational cost, such as the IMSRG(3)-N^7. We note that the IMSRG(3) is not able to achieve as small of errors for these harder Hamiltonians as it is able to achieve for the EM 1.8 Hamiltonian with errors of up to 0.6% in the correlation energy. This suggests that the many-body expansion in the IMSRG converges more slowly when using harder Hamil-

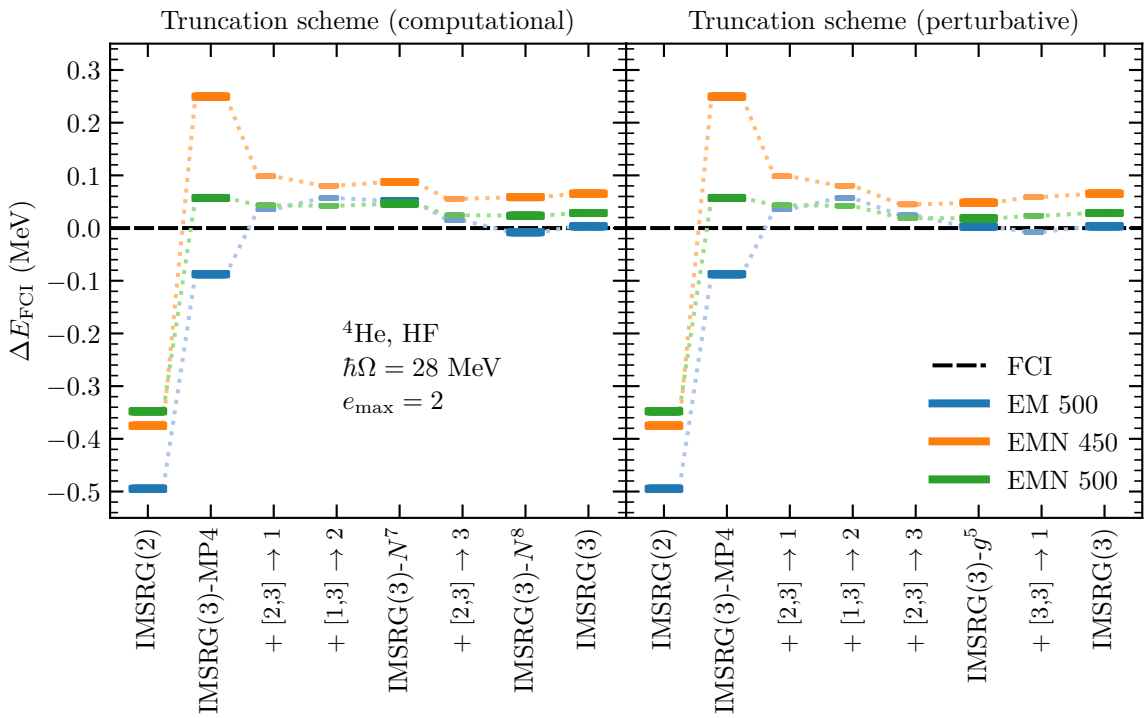

FIG. 9. Differences of ground-state energies of ^{4}He obtained in various truncation schemes to exact FCI results using several unevolved chiral Hamiltonians (see text for details) and an HF reference state following the computational (left panel) and perturbative (right panel) truncation ordering for the fundamental commutators. Thicker, darker bars correspond to the major truncations summarized in Table II. Thinner, lighter bars correspond to intermediate truncations where a single fundamental commutator has been added relative to the truncation scheme to the left.

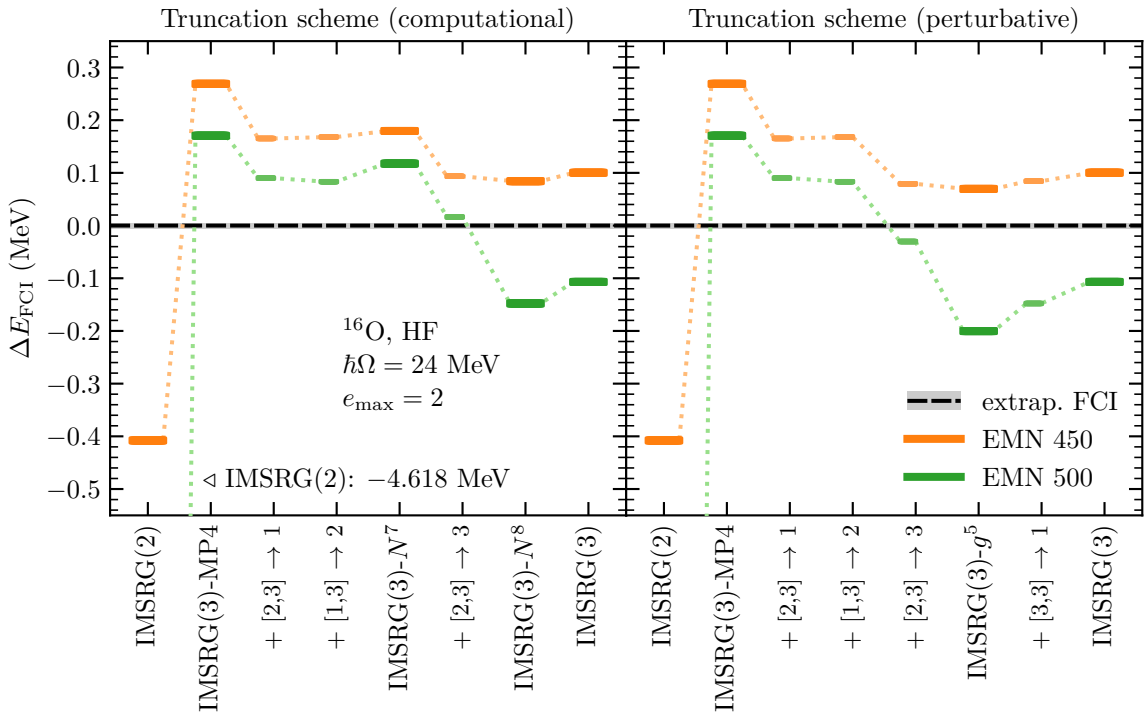

FIG. 10. Same as Fig. 9 but for ^{16}O.

tonians (as one would also expect from perturbative arguments). Still, the convergence behavior of the IMSRG many-body expansion is systematic in the cases discussed here, and the general trends discussed in Sec. IV D continue to hold.

V. SUMMARY AND OUTLOOK

We performed the first systematic study of the inclusion of three-body operators in the IMSRG in small model spaces. To this end, we presented the fundamental commutators, the basic computational building blocks for the IMSRG, required for the IMSRG(3) approximation and introduced new truncations that include subsets of these commutators to understand if one can reliably approximate the IMSRG(3). We applied the full and approximate IMSRG(3) truncations to the closed-shell ^{4}He and ^{16}O using NN-only and NN+3N chiral Hamiltonians with the Hartree-Fock and natural orbital single-particle bases.

When considering NN-only systems, we compared the IMSRG(2) and IMSRG(3) results to exact results in the same model space obtained from FCI calculations for ^{4}He and from extrapolated FCI for ^{16}O. We found that the IMSRG(3) error to the (extrapolated) FCI correlation energy was consistently about 0.3% for the softest Hamiltonian considered and up to 0.6% for harder Hamiltonians. Moreover, the IMSRG(3) results improved systematically over the IMSRG(2) results, where the error to the (extrapolated) FCI results varied quite significantly for different bases and systems. This suggests that the many-body expansion in the IMSRG, which we have taken to the three-body-operator level in this work, is well behaved.

We also considered the performance of various lower-cost approximate IMSRG(3) truncations relative to the full IMSRG(3) approximation. We used the perturbative analysis of Ref. [15] to investigate the expected size of contributions of terms that are included in certain truncations and neglected in others. We found that this perturbative analysis was able to explain the size of contributions to the ground-state energy by individual terms quite well. As a result, the energies calculated using approximate IMSRG(3) truncations that included commutators based on their estimated perturbative importance systematically converged to the full IMSRG(3) result. The major truncation we considered in this approach, the IMSRG(3)-g^5, reproduced the full IMSRG(3) results with very small errors for both NN-only and NN+3N Hamiltonians across all frequencies, single-particle bases, and systems considered.

We also considered the organization of IMSRG(3) truncations based on computational cost. The key major truncation of this approach, the IMSRG(3)-N^7, has a lower computational cost than the IMSRG(3)-g^5 truncation. The IMSRG(3)-N^7 truncation generally saw smaller errors relative to the full IMSRG(3) than the IMSRG(2), but the large contributions of missing commutators prevented its performance from being as good as that of the IMSRG(3)-g^5 truncation. The energy range given by the results from these two major IMSRG(3) truncation schemes (IMSRG(3)-N^7 and IMSRG(3)-g^5) contained the full IMSRG(3) result in all of the cases we studied.

These IMSRG(3) approximations offer possibilities for performing approximate IMSRG(3) calculations where full IMSRG(3) calculations are no longer feasible and for studying the theoretical uncertainty due to the many-body truncation in IMSRG calculations. The challenge going from here is the implementation of full and approximate IMSRG(3) calculations for model spaces where nuclear Hamiltonians are converged. To achieve this, truncations in the three-body model space will need to be imposed in addition to approximations to the IMSRG(3) truncation explored in this work. In Ref. [58], the natural orbitals are used to truncate the three-body model space in a way that accelerates convergence with respect to the employed model-space size. The exploration of different three-body model-space truncations like this will be a key part of future work in the direction of reaching converged IMSRG(3) calculations.

ACKNOWLEDGMENTS

We thank S. R. Stroberg for numerical checks to validate our implementation, P. Arthuis, H. Hergert, S. R. Stroberg, and J. M. Yao for useful discussions, and L. Zurek for comments on the manuscript. This work was supported in part by the Deutsche Forschungsgemeinschaft (DFG, German Research Foundation) – Project-ID 279384907 – SFB 1245 and by the Max Planck Society.

Appendix A: IMSRG(3) flow equations

The uncoupled (or m-scheme) IMSRG(3) flow equations are given by

$$\begin{aligned}\frac{dE}{ds} &= \sum_{pq}(n_p\bar{n}_q - \bar{n}_p n_q)\,\eta_{pq}f_{qp} + \frac{1}{4}\sum_{pqrs}(n_p n_q \bar{n}_r \bar{n}_s - \bar{n}_p\bar{n}_q n_r n_s)\,\eta_{pqrs}\Gamma_{rspq} \\ &\quad + \frac{1}{36}\sum_{pqrstu}(n_p n_q n_r \bar{n}_s \bar{n}_t \bar{n}_u - \bar{n}_p\bar{n}_q\bar{n}_r n_s n_t n_u)\,\eta_{pqrstu}W_{stupqr}\,,\end{aligned} \tag{A1}$$

$$
\begin{aligned}
\frac{df_{12}}{ds} &= \sum_p \left(\eta_{1p} f_{p2} - f_{1p}\eta_{p2}\right) + \sum_{pq} (n_p\bar{n}_q - \bar{n}_p n_q)\left(\eta_{pq}\Gamma_{1q2p} - f_{pq}\eta_{1q2p}\right) \\
&+ \frac{1}{2}\sum_{pqr} (\bar{n}_p\bar{n}_q n_r + n_p n_q \bar{n}_r)\left(\eta_{1rpq}\Gamma_{pq2r} - \Gamma_{1rpq}\eta_{pq2r}\right) \\
&+ \frac{1}{4}\sum_{pqrs} (n_p n_q \bar{n}_r \bar{n}_s - \bar{n}_p\bar{n}_q n_r n_s)\left(\eta_{pqrs}W_{rs1pq2} - \Gamma_{pqrs}\eta_{rs1pq2}\right) \\
&+ \frac{1}{12}\sum_{pqrst} (n_p n_q n_r \bar{n}_s \bar{n}_t + \bar{n}_p\bar{n}_q\bar{n}_r n_s n_t)\left(\eta_{st1pqr}W_{pqrst2} - W_{st1pqr}\eta_{pqrst2}\right),
\end{aligned} \tag{A2}
$$

$$
\begin{aligned}
\frac{d\Gamma_{1234}}{ds} &= (1-P_{12})\sum_p \left(\eta_{1p}\Gamma_{p234} - f_{1p}\eta_{p234}\right) - (1-P_{34})\sum_p \left(\eta_{p3}\Gamma_{12p4} - f_{p3}\eta_{12p4}\right) \\
&+ \frac{1}{2}\sum_{pq} (\bar{n}_p\bar{n}_q - n_p n_q)\left(\eta_{12pq}\Gamma_{pq34} - \Gamma_{12pq}\eta_{pq34}\right) - (1-P_{12})(1-P_{34})\sum_{pq} (n_p\bar{n}_q - \bar{n}_p n_q)\,\eta_{p23q}\Gamma_{1qp4} \\
&+ \sum_{pq} (n_p\bar{n}_q - \bar{n}_p n_q)\left(\eta_{pq}W_{12q34p} - f_{pq}\eta_{12q34p}\right) \\
&+ \frac{1}{2}(1-P_{12})\sum_{pqr} (\bar{n}_p\bar{n}_q n_r + n_p n_q\bar{n}_r)\left(\eta_{r1pq}W_{pq234r} - \Gamma_{r1pq}\eta_{pq234r}\right) \\
&- \frac{1}{2}(1-P_{34})\sum_{pqr} (\bar{n}_p\bar{n}_q n_r + n_p n_q\bar{n}_r)\left(\eta_{pqr3}W_{12rpq4} - \Gamma_{pqr3}\eta_{12rpq4}\right) \\
&+ \frac{1}{6}\sum_{pqrs} (\bar{n}_p\bar{n}_q\bar{n}_r n_s - n_p n_q n_r \bar{n}_s)\left(\eta_{12spqr}W_{pqr34s} - W_{12spqr}\eta_{pqr34s}\right) \\
&+ \frac{1}{4}(1-P_{12})(1-P_{34})\sum_{pqrs} (n_p n_q\bar{n}_r\bar{n}_s - \bar{n}_p\bar{n}_q n_r n_s)\,\eta_{pq1rs3}W_{rs2pq4}\,,
\end{aligned} \tag{A3}
$$

$$
\begin{aligned}
\frac{dW_{123456}}{ds} &= P(12/3)P(45/6)\sum_p \left(\eta_{3p45}\Gamma_{126p} - \Gamma_{3p45}\eta_{126p}\right) \\
&+ P(12/3)\sum_p \left(\eta_{3p}W_{12p456} - f_{3p}\eta_{12p456}\right) - P(45/6)\sum_p \left(\eta_{p6}W_{12345p} - f_{p6}\eta_{12345p}\right) \\
&+ \frac{1}{2}P(12/3)\sum_{pq} (\bar{n}_p\bar{n}_q - n_p n_q)\left(\eta_{12pq}W_{pq3456} - \Gamma_{12pq}\eta_{pq3456}\right) \\
&- \frac{1}{2}P(45/6)\sum_{pq} (\bar{n}_p\bar{n}_q - n_p n_q)\left(\eta_{pq45}W_{123pq6} - \Gamma_{pq45}\eta_{123pq6}\right) \\
&+ P(12/3)P(45/6)\sum_{pq} (\bar{n}_p n_q - n_p\bar{n}_q)\left(\eta_{3pq6}W_{12q45p} - \Gamma_{3pq6}\eta_{12q45p}\right) \\
&+ \frac{1}{6}\sum_{pqr} (n_p n_q n_r + \bar{n}_p\bar{n}_q\bar{n}_r)\left(\eta_{123pqr}W_{pqr456} - W_{123pqr}\eta_{pqr456}\right) \\
&+ \frac{1}{2}P(12/3)P(45/6)\sum_{pqr} (\bar{n}_p\bar{n}_q n_r + n_p n_q\bar{n}_r)\left(\eta_{pq345r}W_{12rpq6} - W_{pq345r}\eta_{12rpq6}\right),
\end{aligned} \tag{A4}
$$

where the permutation operator P_{pq} exchanges the indices p and q in the following expression. We further define the additional permutation operator $P(pq/r) \equiv 1 - P_{pr} - P_{qr}$. The action of the permutation operators in Eqs. (A3) and (A4) ensures the antisymmetry of two- and three-body matrix elements over the course of the IMSRG evolution. We note that the m-scheme IMSRG(3) flow equations agree with those in Ref. [15], except for the following typo:

1. The occupation numbers in the term on the third row of Eq. (A2) are corrected.

Our expressions differ somewhat because we do not use the Hermiticity of the Hamiltonian and the anti-Hermiticity of the generator to manipulate the terms. We note that there is no possible reduction in the computational cost obtainable by these manipulations. We also provide a list of corrections between our m-scheme IMSRG(3) fundamental commutators and those in Ref. [15]:

1. Our expression for the $[1,3] \to 2$ commutator has an overall factor of $1/4$ relative to that of Ref. [15].
2. We include an additional term in the $[2,3] \to 3$ commutator that was missing in Ref. [15].
3. We provide an expression for the $[2,3] \to 2$ commutator that is generally valid. The expression given in Ref. [15] is valid only when one of A and B is Hermitian and the other is anti-Hermitian.

Appendix B: Spherical fundamental commutators

In practice, the IMSRG(3) framework is applied to closed-shell systems with a spherical reference state. Given the shared rotational symmetry of the reference state and nuclear Hamiltonians, one can choose a spherical single-particle basis and use angular-momentum-coupling techniques to significantly reduce the storage and computational cost of the IMSRG(3) solution.

1. Primer on angular-momentum coupling

We offer a brief introduction to the concepts of angular-momentum coupling and the associated notation. For a more detailed treatment of the formalism of angular-momentum coupling, we refer readers to Refs. [59, 60].

The single-particle basis is chosen to consist of spherical states

$$|p\rangle \equiv |\xi_p j_p m_p\rangle \equiv |\tilde{p} m_p\rangle \,, \tag{B1}$$

with the total angular momentum j_p, the angular-momentum projection m_p, and the remaining quantum numbers that characterize the state ξ_p. In nuclear applications, $\xi = (n, l, t)$, with the radial quantum number n, the orbital angular momentum l, and the isospin projection t. The reduced single-particle index $\tilde{p}$ is a collective index for all the quantum numbers of the state besides m_p and always has an associated j_p. These spherical states are eigenstates of the one-body total angular momentum squared J^2 and the z projection of the one-body total angular momentum J_z.

When using a spherical single-particle basis, the one-body matrix elements of operators that are scalars under rotations in space and spin (as is the case for the Hamiltonian and the generator in the IMSRG),

$$\langle \xi_p j_p m_p | O | \xi_q j_q m_q \rangle = \langle \tilde{p} m_p | O | \tilde{q} m_q \rangle \,, \tag{B2}$$

are diagonal in $j_p = j_q \equiv J_O$ and in $m_p = m_q \equiv M_O$ and independent of M_O. This allows for the compact representation of the one-body matrix elements as

$$O^{J_O}_{\tilde{p}\tilde{q}} \equiv \langle \xi_p, j_p = J_O, m_p = j_p | O | \xi_q, j_q = J_O, m_q = j_q \rangle \,, \tag{B3}$$

where the single-particle indices now only run over reduced indices. We have introduced a channel notation where the superscript J_O indicates that the matrix elements are partitioned into channels where matrix elements in each channel are nonzero only when $j_p = j_q = J_O$. While it is conventional to use j, J, and $\mathcal{J}$ for one-, two-, and three-body angular momenta, respectively, we opt instead to use j only for single-particle angular momenta and J for all angular momenta that appear in one-, two-, and three-body angular-momentum channels.

The antisymmetric two-body states

$$|pq\rangle \equiv a_p^\dagger a_q^\dagger |0\rangle \tag{B4}$$

may be coupled to two-body total angular momentum J using the Clebsch-Gordan coefficients

$$C^{JM}_{j_p m_p j_q m_q} = \langle (\tilde{p}\tilde{q}) JM | pq \rangle \,, \tag{B5}$$

yielding the coupled two-body states

$$|(\tilde{p}\tilde{q}) JM\rangle = \sum_{m_p m_q} C^{JM}_{j_p m_p j_q m_q} |pq\rangle \,, \tag{B6}$$

which are eigenstates of two-body J^2 and J_z.

When using coupled two-body states, the two-body matrix elements of scalars under rotations in space and spin,

$$\langle (\tilde{p}\tilde{q}) J_{pq} M_{pq} | O | (\tilde{r}\tilde{s}) J_{rs} M_{rs} \rangle \,, \tag{B7}$$

are diagonal in $J_{pq} = J_{rs} \equiv J_O$ and in $M_{pq} = M_{rs} \equiv M_O$ and independent of M_O. This allows for the compact representation of these coupled matrix elements as

$$O^{J_O}_{\tilde{p}\tilde{q}\tilde{r}\tilde{s}} \equiv \langle (\tilde{p}\tilde{q}) J_{pq} = J_O, M_{pq} = J_{pq} | O | (\tilde{r}\tilde{s}) J_{rs} = J_O, M_{rs} = J_{rs} \rangle \,, \tag{B8}$$

where the single-particle indices again only run over reduced indices, and the matrix elements have a channel structure that specifies to which total angular momentum J_O the bra and ket states are coupled.

This approach is quickly extended to three-body states

$$|pqr\rangle \equiv a_p^\dagger a_q^\dagger a_r^\dagger |0\rangle \,, \tag{B9}$$

where the angular momenta j_p and j_q are coupled to an intermediate two-body angular momentum J_{pq} that is then coupled with j_r to the three-body angular momentum J, yielding the coupled three-body states

$$|[(\tilde{p}\tilde{q})J_{pq}\tilde{r}]JM\rangle = \sum_{m_p m_q M_{pq} m_r} C^{J_{pq} M_{pq}}_{j_p m_p j_q m_q} C^{JM}_{J_{pq} M_{pq} j_r m_r} \, |pqr\rangle \,, \tag{B10}$$

which are eigenstates of the three-body J^2 and J_z. Here, we made a choice to couple the p and q indices first and then the r index. One could also couple two different indices in the first coupling step and then couple the remaining index last to arrive at valid eigenstates of J^2 and J_z. One arrives at a similar representation for the coupled three-body matrix elements of a scalar operator,

$$O^{(J_O, J_{pq}, J_{st})}_{\tilde{p}\tilde{q}\tilde{r}\tilde{s}\tilde{t}\tilde{u}} \equiv \langle [(\tilde{p}\tilde{q})J_{pq}\tilde{r}]J_{pqr} = J_O, M_{pqr} = J_{pqr} | O | [(\tilde{s}\tilde{t})J_{st}\tilde{u}]J_{stu} = J_O, M_{stu} = J_{stu} \rangle \,, \tag{B11}$$

with $J_O = J_{pqr} = J_{stu}$ and $M_{pqr} = M_{stu}$. The channel structure of three-body coupled matrix elements is complicated by the appearance of the intermediate couplings J_{pq} and J_{st}, which do not have to be equal.

Angular-momentum coupling allows one to reduce the working equations of a theory to expressions that depend only on the coupled matrix elements discussed above. The substantial reduction in storage requirements due to working with coupled matrix elements and in computational cost by having any purely geometric dependence on angular-momentum projection analytically simplified is essential to making IMSRG(3) calculations tractable.

For this work, we used the automated angular-momentum-coupling tool AMC [61] to generate coupled expressions for the fundamental commutators. The generated expressions and their implementations were validated by evaluating the coupled and uncoupled implementations for the same input and observing that the same coupled matrix elements were produced.

2. Coupled expressions for fundamental commutators

In the following, we present the coupled expressions for the fundamental commutators required for the IMSRG(3). We drop the tilde from reduced single-particle indices, as all matrix elements are coupled matrix elements, and thus all indices on the matrix elements are reduced single-particle indices.

The expressions are nonantisymmetrized, so the resulting two- and three-body coupled matrix elements must be antisymmetrized by applying the appropriate antisymmetrizer to the bra and ket indices. The antisymmetrization of two-body bra indices is given by

$$\bar{O}^{J_O}_{pqrs} \equiv \mathcal{A}_2 O^{J_O}_{pqrs} = \frac{1}{2}\left[O^{J_O}_{pqrs} - (-1)^{j_p + j_q - J_O} O^{J_O}_{qprs} \right], \tag{B12}$$

where $\mathcal{A}_2$ is the two-body antisymmetrizer and the output matrix elements $\bar{O}^{J_O}_{pqrs}$ are antisymmetric under exchange of p and q. If the input matrix elements $O^{J_O}_{pqrs}$ are already antisymmetric in p and q, the antisymmetrization does nothing and the input and output matrix elements are identical. Similarly, the antisymmetrization of two-body ket indices is given by

$$\bar{O}^{J_O}_{pqrs} \equiv O^{J_O}_{pqrs} \mathcal{A}_2 = \frac{1}{2}\left[O^{J_O}_{pqrs} - (-1)^{j_r + j_s - J_O} O^{J_O}_{pqsr} \right]. \tag{B13}$$

The antisymmetrization of three-body bra indices is given by

$$\begin{aligned}\bar{O}^{(J_O,J_{pq},J_{st})}_{pqrstu} \equiv \mathcal{A}_3 O^{(J_O,J_{pq},J_{st})}_{pqrstu} = \frac{1}{6}\Bigg[& O^{(J_O,J_{pq},J_{st})}_{pqrstu} + \hat{J}_{pq}\sum_{J_2}\hat{J}_2 \begin{Bmatrix} j_p & j_q & J_{pq} \\ j_r & J_O & J_2 \end{Bmatrix} O^{(J_O,J_2,J_{st})}_{rqpstu} \\ & - (-1)^{j_q+j_r-J_{pq}}\hat{J}_{pq}\sum_{J_2}(-1)^{J_2}\hat{J}_2 \begin{Bmatrix} j_q & j_p & J_{pq} \\ j_r & J_O & J_2 \end{Bmatrix} O^{(J_O,J_2,J_{st})}_{prqstu} \\ & - (-1)^{j_p+j_q-J_{pq}}\hat{J}_{pq}\sum_{J_2}\hat{J}_2 \begin{Bmatrix} j_q & j_p & J_{pq} \\ j_r & J_O & J_2 \end{Bmatrix} O^{(J_O,J_2,J_{st})}_{rpqstu} \\ & - (-1)^{j_q+j_r}\hat{J}_{pq}\sum_{J_2}(-1)^{J_2}\hat{J}_2 \begin{Bmatrix} j_p & j_q & J_{pq} \\ j_r & J_O & J_2 \end{Bmatrix} O^{(J_O,J_2,J_{st})}_{qrpstu} - (-1)^{j_p+j_q-J_{pq}} O^{(J_O,J_{pq},J_{st})}_{qprstu}\Bigg], \end{aligned} \tag{B14}$$

with the three-body antisymmetrizer $\mathcal{A}_3$, $\hat{J} \equiv \sqrt{2J+1}$, and the Wigner $6j$ symbols

$$\begin{Bmatrix} j_1 & j_2 & j_3 \\ j_4 & j_5 & j_6 \end{Bmatrix}.$$

The antisymmetrization of three-body ket indices is given by

$$\begin{aligned}\bar{O}^{(J_O,J_{pq},J_{st})}_{pqrstu} \equiv O^{(J_O,J_{pq},J_{st})}_{pqrstu}\mathcal{A}_3 = \frac{1}{6}\Bigg[& O^{(J_O,J_{pq},J_{st})}_{pqrstu} + \hat{J}_{st}\sum_{J_2}\hat{J}_2 \begin{Bmatrix} j_s & j_t & J_{st} \\ j_u & J_O & J_2 \end{Bmatrix} O^{(J_O,J_{pq},J_2)}_{pqruts} \\ & - (-1)^{j_t+j_u-J_{st}}\hat{J}_{st}\sum_{J_2}(-1)^{J_2}\hat{J}_2 \begin{Bmatrix} j_t & j_s & J_{st} \\ j_u & J_O & J_2 \end{Bmatrix} O^{(J_O,J_{pq},J_2)}_{pqrsut} \\ & - (-1)^{j_s+j_t-J_{st}}\hat{J}_{st}\sum_{J_2}\hat{J}_2 \begin{Bmatrix} j_t & j_s & J_{st} \\ j_u & J_O & J_2 \end{Bmatrix} O^{(J_O,J_{pq},J_2)}_{pqrust} \\ & - (-1)^{j_t+j_u}\hat{J}_{st}\sum_{J_2}(-1)^{J_2}\hat{J}_2 \begin{Bmatrix} j_s & j_t & J_{st} \\ j_u & J_O & J_2 \end{Bmatrix} O^{(J_O,J_{pq},J_2)}_{pqrtus} - (-1)^{j_s+j_t-J_{st}} O^{(J_O,J_{pq},J_{st})}_{pqrtsu}\Bigg]. \end{aligned} \tag{B15}$$

a. $[1,1] \to \circ$

$$C^{J_C}_{12} = \sum_p \left(A^{J_C}_{1p} B^{J_C}_{p2} - B^{J_C}_{1p} A^{J_C}_{p2} \right), \tag{B16}$$

$$C^{(0)} = \sum_{J_p} \hat{J}_p^2 \sum_{pq} (n_p \bar{n}_q - \bar{n}_p n_q) A^{J_p}_{pq} B^{J_p}_{qp}\,. \tag{B17}$$

b. $[1,2] \to \circ$

$$C^{J_C}_{1234} = 2\sum_{J_A}\sum_p \left(A^{J_A}_{1p} B^{J_C}_{p234} - A^{J_A}_{p3} B^{J_C}_{12p4} \right), \tag{B18}$$

$$C^{J_C}_{12} = \frac{1}{\hat{J}_C^2}\sum_{J_B}\hat{J}_B^2 \sum_{J_A}\sum_{pq} (n_p \bar{n}_q - \bar{n}_p n_q) A^{J_A}_{pq} B^{J_B}_{1q2p}\,. \tag{B19}$$

c. $[2,2] \to \circ$

$$C^{(J_C,J_{12},J_{45})}_{123456} = -9\hat{J}_{12}\hat{J}_{45}\sum_p \begin{Bmatrix} j_3 & j_p & J_{45} \\ j_6 & J_C & J_{12} \end{Bmatrix} \left(A^{J_{45}}_{3p45} B^{J_{12}}_{126p} - B^{J_{45}}_{3p45} A^{J_{12}}_{126p} \right), \tag{B20}$$

$$C^{J_C}_{1234} = D^{J_C}_{1234} + E^{J_C}_{1234}\,, \tag{B21}$$

$$D^{J_C}_{1234} = \frac{1}{2}\sum_{pq} (\bar{n}_p\bar{n}_q - n_p n_q) \left(A^{J_C}_{12pq} B^{J_C}_{pq34} - B^{J_C}_{12pq} A^{J_C}_{pq34} \right), \tag{B22}$$

$$\overline{E}^{J'_C}_{1432} = 4\sum_{pq} (n_p\bar{n}_q - \bar{n}_p n_q) \overline{A}^{J'_C}_{pq32} \overline{B}^{J'_C}_{14pq}\,, \tag{B23}$$

$$C^{J_C}_{12} = \frac{1}{2}\frac{1}{\hat{J}^2_C}\sum_{J_{pq}} \hat{J}^2_{pq} \sum_{pqr} (\bar{n}_p\bar{n}_q n_r + n_p n_q \bar{n}_r) \left(A^{J_{pq}}_{1rpq} B^{J_{pq}}_{pq2r} - B^{J_{pq}}_{1rpq} A^{J_{pq}}_{pq2r} \right), \tag{B24}$$

$$C^{(0)} = \frac{1}{4}\sum_{J_{pq}} \hat{J}^2_{pq} \sum_{pq} (n_p n_q \bar{n}_r \bar{n}_s - \bar{n}_p\bar{n}_q n_r n_s) A^{J_{pq}}_{pqrs} B^{J_{pq}}_{rspq}\,, \tag{B25}$$

where we split the $[2,2] \to 2$ commutator in Eq. (B21) into two terms, Eq. (B22) and Eq. (B23). The matrix elements of $A^{(2)}$ and $B^{(2)}$ in Eq. (B23) (the $\overline{A}$ and $\overline{B}$ objects) are obtained by a Pandya transformation [62],

$$\overline{O}^{J'_O}_{1432} \equiv -\sum_{J_O} \hat{J}^2_O \begin{Bmatrix} j_1 & j_4 & J'_O \\ j_3 & j_2 & J_O \end{Bmatrix} O^{J_O}_{1234}\,. \tag{B26}$$

The Pandya transformation is its own inverse, so the output Pandya-transformed matrix elements in Eq. (B23) ($\overline{E}^{J'_C}_{1432}$) must be Pandya transformed again to arrive at the standard coupled matrix elements ($E^{J_C}_{1234}$) that contribute in Eq. (B21) to obtain the full $[2,2] \to 2$ commutator result.

d. $[1,3] \to \circ$

$$C^{(J_C,J_{12},J_{45})}_{123456} = 3\sum_{J_A}\sum_p \left[A^{J_A}_{3p} B^{(J_C,J_{12},J_{45})}_{12p456} - A^{J_A}_{p6} B^{(J_C,J_{12},J_{45})}_{12345p} \right], \tag{B27}$$

$$C^{J_C}_{1234} = \frac{1}{\hat{J}^2_C}\sum_{J_B} \hat{J}^2_B \sum_{J_A}\sum_{pq} (n_p\bar{n}_q - \bar{n}_p n_q) A^{J_A}_{pq} B^{(J_B,J_C,J_C)}_{12q34p}\,. \tag{B28}$$

e. $[2,3] \to \circ$

$$C^{(J_C,J_{12},J_{45})}_{123456} = D^{(J_C,J_{12},J_{45})}_{123456} + E^{(J_C,J_{12},J_{45})}_{123456}\,, \tag{B29}$$

$$D^{(J_C,J_{12},J_{45})}_{123456} = \frac{3}{2}\sum_{pq} (\bar{n}_p\bar{n}_q - n_p n_q) \left[A^{J_{12}}_{12pq} B^{(J_C,J_{12},J_{45})}_{pq3456} - A^{J_{45}}_{pq45} B^{(J_C,J_{12},J_{45})}_{123pq6} \right], \tag{B30}$$

$$\begin{aligned} E^{(J_C,J_{12},J_{45})}_{123456} = 9 \sum_{J_A,J_B,J_{qp}} & (-1)^{J_B+J_C} \hat{J}^2_A \hat{J}^2_B \hat{J}^2_{qp} \sum_{pq} (\bar{n}_p n_q - n_p\bar{n}_q)(-1)^{j_3+j_q} \\ & \times \begin{Bmatrix} j_6 & j_3 & J_{qp} \\ j_p & j_q & J_A \end{Bmatrix} \begin{Bmatrix} J_{12} & J_{45} & J_{qp} \\ j_p & j_q & J_B \end{Bmatrix} \begin{Bmatrix} J_{qp} & J_{12} & J_{45} \\ J_C & j_6 & j_3 \end{Bmatrix} A^{J_A}_{3pq6} B^{(J_B,J_{12},J_{45})}_{12q45p}\,, \end{aligned} \tag{B31}$$

$$\begin{aligned} C^{J_C}_{1234} = -\frac{(-1)^{J_C}}{\hat{J}_C} & \sum_{J_{pq},J_B} \hat{J}_{pq} \hat{J}^2_B \sum_{pqr} (\bar{n}_p\bar{n}_q n_r + n_p n_q \bar{n}_r) \\ & \times \left[(-1)^{j_1+j_2} \begin{Bmatrix} j_2 & j_1 & J_C \\ j_r & J_B & J_{pq} \end{Bmatrix} A^{J_{pq}}_{r1pq} B^{(J_B,J_{pq},J_C)}_{pq234r} - (-1)^{j_3+j_4} \begin{Bmatrix} j_4 & j_3 & J_C \\ j_r & J_B & J_{pq} \end{Bmatrix} A^{J_{pq}}_{pqr3} B^{(J_B,J_C,J_{pq})}_{12rpq4} \right], \end{aligned} \tag{B32}$$

$$C^{J_C}_{12} = \frac{1}{4}\frac{1}{\hat{J}^2_C}\sum_{J_{pq},J_B}\hat{J}^2_B\sum_{pqrs}(n_p n_q \bar{n}_r \bar{n}_s - \bar{n}_p\bar{n}_q n_r n_s)A^{J_{pq}}_{pqrs}B^{(J_B,J_{pq},J_{pq})}_{rs1pq2}\,, \tag{B33}$$

where we split the $[2,3]\to 3$ commutator in Eq. (B29) into two terms.

f. $[3,3]\to\circ$

$$C^{(J_C,J_{12},J_{45})}_{123456} = D^{(J_C,J_{12},J_{45})}_{123456} + E^{(J_C,J_{12},J_{45})}_{123456}\,, \tag{B34}$$

$$D^{(J_C,J_{12},J_{45})}_{123456} = \frac{1}{6}\sum_{J_{pq}}\sum_{pqr}(n_p n_q n_r + \bar{n}_p\bar{n}_q\bar{n}_r)\left[A^{(J_C,J_{12},J_{pq})}_{123pqr}B^{(J_C,J_{pq},J_{45})}_{pqr456} - B^{(J_C,J_{12},J_{pq})}_{123pqr}A^{(J_C,J_{pq},J_{45})}_{pqr456}\right], \tag{B35}$$

$$\overline{E}^{(J'_C,J_{12},J_{45})}_{126453} = \frac{9}{2}\sum_{J_{pq}}\sum_{pqr}(\bar{n}_p\bar{n}_q n_r + n_p n_q\bar{n}_r)\left[\overline{A}^{(J'_C,J_{pq},J_{45})}_{pqr453}\overline{B}^{(J'_C,J_{12},J_{pq})}_{126pqr} - \overline{B}^{(J'_C,J_{pq},J_{45})}_{pqr453}\overline{A}^{(J'_C,J_{12},J_{pq})}_{126pqr}\right], \tag{B36}$$

$$C^{J_C}_{1234} = D^{J_C}_{1234} + E^{J_C}_{1234}\,, \tag{B37}$$

$$D^{J_C}_{1234} = \frac{1}{6}\frac{1}{\hat{J}^2_C}\sum_{J_{pqr}}\hat{J}^2_{pqr}\sum_{J_{pq}}\sum_{pqrs}(\bar{n}_p\bar{n}_q\bar{n}_r n_s - n_p n_q n_r\bar{n}_s)\left[A^{(J_{pqr},J_C,J_{pq})}_{12spqr}B^{(J_{pqr},J_{pq},J_C)}_{pqr34s} - B^{(J_{pqr},J_C,J_{pq})}_{12spqr}A^{(J_{pqr},J_{pq},J_C)}_{pqr34s}\right], \tag{B38}$$

$$\begin{aligned}E^{J_C}_{1234} = {}& -(-1)^{j_1+j_3+J_C}\sum_{J_A,J_B}\hat{J}^2_A\hat{J}^2_B(-1)^{J_A+J_B}\sum_{J_{pq},J_{rs}}\sum_{J_2}\hat{J}^2_2\sum_{pqrs}(n_p n_q\bar{n}_r\bar{n}_s - \bar{n}_p\bar{n}_q n_r n_s)\\ &\times\begin{Bmatrix}J_{pq} & J_{rs} & J_2\\ j_3 & j_1 & J_A\end{Bmatrix}\begin{Bmatrix}J_{pq} & J_{rs} & J_2\\ j_2 & j_4 & J_B\end{Bmatrix}\begin{Bmatrix}j_3 & j_4 & J_C\\ j_2 & j_1 & J_2\end{Bmatrix}A^{(J_A,J_{pq},J_{rs})}_{pq1rs3}B^{(J_B,J_{rs},J_{pq})}_{rs2pq4}\,,\end{aligned} \tag{B39}$$

$$C^{J_C}_{12} = \frac{1}{12}\frac{1}{\hat{J}^2_C}\sum_{J_{pqr},J_{pq},J_{st}}\hat{J}^2_{pqr}\sum_{pqrst}(n_p n_q n_r\bar{n}_s\bar{n}_t + \bar{n}_p\bar{n}_q\bar{n}_r n_s n_t)\left[A^{(J_{pqr},J_{st},J_{pq})}_{st1pqr}B^{(J_{pqr},J_{pq},J_{st})}_{pqrst2} - B^{(J_{pqr},J_{st},J_{pq})}_{st1pqr}A^{(J_{pqr},J_{pq},J_{st})}_{pqrst2}\right], \tag{B40}$$

$$C^{(0)} = \frac{1}{36}\sum_{J_{pqr},J_{pq},J_{st}}\hat{J}^2_{pqr}\sum_{pqrstu}(n_p n_q n_r\bar{n}_s\bar{n}_t\bar{n}_u - \bar{n}_p\bar{n}_q\bar{n}_r n_s n_t n_u)A^{(J_{pqr},J_{pq},J_{st})}_{pqrstu}B^{(J_{pqr},J_{st},J_{pq})}_{stupqr}\,. \tag{B41}$$

Here we split the $[3,3]\to 3$ commutator in Eq. (B34) and the $[3,3]\to 2$ commutator in Eq. (B37) each into two terms. The matrix elements of $A^{(3)}$ and $B^{(3)}$ in Eq. (B36) (the $\overline{A}$ and $\overline{B}$ objects) are obtained by the three-body analog of the Pandya transformation,

$$\overline{O}^{(J'_O,J_{12},J_{45})}_{126453} \equiv -\sum_{J_O}\hat{J}^2_O\begin{Bmatrix}J_{12} & j_6 & J'_O\\ J_{45} & j_3 & J_O\end{Bmatrix}O^{(J_O,J_{12},J_{45})}_{123456}\,. \tag{B42}$$

The output Pandya-transformed matrix elements in Eq. (B36) must be Pandya transformed again to arrive at the standard matrix elements that contribute in Eq. (B34) to obtain the full $[3,3]\to 3$ commutator result.

[1] K. Hebeler, J. D. Holt, J. Menéndez, and A. Schwenk, "Nuclear Forces and Their Impact on Neutron-Rich Nuclei and Neutron-Rich Matter," Annu. Rev. Nucl. Part. Sci. **65**, 457 (2015).

[2] T. D. Morris, J. Simonis, S. R. Stroberg, C. Stumpf, G. Hagen, J. D. Holt, G. R. Jansen, T. Papenbrock, R. Roth, and A. Schwenk, "Structure of the Lightest Tin Isotopes," Phys. Rev. Lett. **120**, 152503 (2018).

[3] H. Hergert, "A Guided Tour of ab initio Nuclear Many-Body Theory," Front. Phys. **8**, 379 (2020).

[4] E. Epelbaum, H.-W. Hammer, and U.-G. Meißner, "Modern theory of nuclear forces," Rev. Mod. Phys. **81**, 1773 (2009).

[5] R. Machleidt and D. R. Entem, "Chiral effective field theory and nuclear forces," Phys. Rep. **503**, 1 (2011).

[6] K. Hebeler, S. K. Bogner, R. J. Furnstahl, A. Nogga, and A. Schwenk, "Improved nuclear matter calculations from chiral low-momentum interactions," Phys. Rev. C **83**, 031301(R) (2011).

[7] A. Ekström, G. R. Jansen, K. A. Wendt, G. Hagen, T. Papenbrock, B. D. Carlsson, C. Forssén, M. Hjorth-Jensen, P. Navrátil, and W. Nazarewicz, "Accurate nuclear radii and binding energies from a chiral interaction," Phys. Rev. C **91**, 051301(R) (2015).

[8] D. R. Entem, R. Machleidt, and Y. Nosyk, "High-quality two-nucleon potentials up to fifth order of the chiral expansion," Phys. Rev. C **96**, 024004 (2017).

[9] E. Epelbaum, H. Krebs, and P Reinert, "High-Precision Nuclear Forces From Chiral EFT: State-of-the-Art, Challenges, and Outlook," Front. Phys. **8**, 98 (2020).

[10] K. Hebeler, "Three-nucleon forces: Implementation and applications to atomic nuclei and dense matter," Phys. Rep. **890**, 1

(2021).
[11] W. G. Jiang, A. Ekström, C. Forssén, G. Hagen, G. R. Jansen, and T. Papenbrock, "Accurate bulk properties of nuclei from $A = 2$ to ∞ from potentials with Δ isobars," Phys. Rev. C **102**, 054301 (2020).
[12] G. Hagen, T. Papenbrock, M. Hjorth-Jensen, and D. J. Dean, "Coupled-cluster computations of atomic nuclei," Rep. Prog. Phys. **77**, 096302 (2014).
[13] S. Binder, J. Langhammer, A. Calci, and R. Roth, "Ab initio path to heavy nuclei," Phys. Lett. B **736**, 119 (2014).
[14] K. Tsukiyama, S. K. Bogner, and A. Schwenk, "In-medium Similarity Renormalization Group for Nuclei," Phys. Rev. Lett. **106**, 222502 (2011).
[15] H. Hergert, S. K. Bogner, T. D. Morris, A. Schwenk, and K. Tsukiyama, "The In-Medium Similarity Renormalization Group: A novel ab initio method for nuclei," Phys. Rep. **621**, 165 (2016).
[16] S. R. Stroberg, H. Hergert, S. K. Bogner, and J. D. Holt, "Nonempirical Interactions for the Nuclear Shell Model: An Update," Annu. Rev. Nucl. Part. Sci. **69**, 307 (2019).
[17] W. H. Dickhoff and C. Barbieri, "Self-consistent Green's function method for nuclei and nuclear matter," Prog. Part. Nucl. Phys. **52**, 377 (2004).
[18] V. Somà, P. Navrátil, F. Raimondi, C. Barbieri, and T. Duguet, "Novel chiral Hamiltonian and observables in light and medium-mass nuclei," Phys. Rev. C **101**, 014318 (2020).
[19] J. D. Holt, J. Menéndez, J. Simonis, and A. Schwenk, "Three-nucleon forces and spectroscopy of neutron-rich calcium isotopes," Phys. Rev. C **90**, 024312 (2014).
[20] A. Tichai, J. Langhammer, S. Binder, and R. Roth, "Hartree-Fock many-body perturbation theory for nuclear ground-states," Phys. Lett. B **756**, 283 (2016).
[21] A. Tichai, P. Arthuis, T. Duguet, H. Hergert, V. Somá, and R. Roth, "Bogoliubov many-body perturbation theory for open-shell nuclei," Phys. Lett. B **786**, 195 (2018).
[22] A. Tichai, R Roth, and T. Duguet, "Many-Body Perturbation Theories for Finite Nuclei," Front. Phys. **8**, 164 (2020).
[23] Y. S. Lee, S. A. Kucharski, and R. J. Bartlett, "A coupled cluster approach with triple excitations," J. Chem. Phys. **81**, 5906 (1984).
[24] J. Noga and R. J. Bartlett, "The full CCSDT model for molecular electronic structure," J. Chem. Phys. **86**, 7041 (1987).
[25] G. E. Scuseria and H. F. Schaefer, "A new implementation of the full CCSDT model for molecular electronic structure," Chem. Phys. Lett. **152**, 382 (1988).
[26] P. Piecuch and M. Włoch, "Renormalized coupled-cluster methods exploiting left eigenstates of the similarity-transformed Hamiltonian," J. Chem. Phys. **123**, 224105 (2005).
[27] A. G. Taube and R. J. Bartlett, "Improving upon CCSD(T): ΛCCSD(T). I. Potential energy surfaces," J. Chem. Phys. **128**, 044110 (2008).
[28] S. Binder, P. Piecuch, A. Calci, J. Langhammer, P. Navrátil, and R. Roth, "Extension of coupled-cluster theory with a noniterative treatment of connected triply excited clusters to three-body Hamiltonians," Phys. Rev. C **88**, 054319 (2013).
[29] G. Hagen, G. R. Jansen, and T. Papenbrock, "Structure of ^{78}Ni From First-Principles Computations," Phys. Rev. Lett. **117**, 172501 (2016).
[30] M. Miorelli, S. Bacca, G. Hagen, and T. Papenbrock, "Computing the dipole polarizability of ^{48}Ca with increased precision," Phys. Rev. C **98**, 014324 (2018).
[31] S. Kaufmann, J. Simonis, S. Bacca, J. Billowes, M. L. Bissell, K. Blaum, *et al.*, "Charge Radius of the Short-Lived ^{68}Ni and Correlation with the Dipole Polarizability," Phys. Rev. Lett. **124**, 132502 (2020).
[32] S. J. Novario, P. Gysbers, J. Engel, G. Hagen, G. R. Jansen, T. D. Morris, P. Navrátil, T. Papenbrock, and S. Quaglioni, "Coupled-cluster calculations of neutrinoless double-beta decay in ^{48}Ca," arXiv:2008.09696.
[33] J. Simonis, S. R. Stroberg, K. Hebeler, J. D. Holt, and A. Schwenk, "Saturation with chiral interactions and consequences for finite nuclei," Phys. Rev. C **96**, 014303 (2017).
[34] H. Hergert, J. M. Yao, T. D. Morris, N. M. Parzuchowski, S. K. Bogner, and J. Engel, "Nuclear Structure from the In-Medium Similarity Renormalization Group," J. Phys. Conf. Ser. **1041**, 012007 (2018).
[35] C. Li and F. A. Evangelista, "Connected three-body terms in single-reference unitary many-body theories: Iterative and perturbative approximations," J. Chem. Phys. **152**, 234116 (2020).
[36] F. Wegner, "Flow-equations for Hamiltonians," Ann. Phys. **506**, 77 (1994).
[37] S. D. Glazek and K. G. Wilson, "Renormalization of Hamiltonians," Phys. Rev. D **48**, 5863 (1993).
[38] S. K. Bogner, R. J. Furnstahl, and R. J. Perry, "Similarity renormalization group for nucleon-nucleon interactions," Phys. Rev. C **75**, 061001(R) (2007).
[39] S. K. Bogner, R. J. Furnstahl, and A. Schwenk, "From low-momentum interactions to nuclear structure," Prog. Part. Nucl. Phys. **65**, 94 (2010).
[40] E. D. Jurgenson, P. Navrátil, and R. J. Furnstahl, "Evolution of Nuclear Many-Body Forces with the Similarity Renormalization Group," Phys. Rev. Lett. **103**, 082501 (2009).
[41] K. Hebeler, "Momentum-space evolution of chiral three-nucleon forces," Phys. Rev. C **85**, 021002(R) (2012).
[42] G. C. Wick, "The Evaluation of the Collision Matrix," Phys. Rev. **80**, 268 (1950).
[43] G. Hagen, T. Papenbrock, D. J. Dean, A. Schwenk, A. Nogga, M. Włoch, and P. Piecuch, "Coupled-cluster theory for three-body Hamiltonians," Phys. Rev. C **76**, 034302 (2007).
[44] R. Roth, S. Binder, K. Vobig, A. Calci, J. Langhammer, and P. Navrátil, "Medium-Mass Nuclei with Normal-Ordered Chiral NN+3N Interactions," Phys. Rev. Lett. **109**, 052501 (2012).
[45] T. D. Morris, *Systematic improvements of ab-initio in-medium similarity renormalization group calculations*, Ph.D. thesis, Michigan State University, East Lansing (2016).
[46] A. Cipollone, C. Barbieri, and P. Navrátil, "Isotopic Chains Around Oxygen from Evolved Chiral Two- and Three-Nucleon Interactions," Phys. Rev. Lett. **111**, 062501 (2013).
[47] J. Zhao and G. E. Scuseria, https://github.com/tschijnmo/drudge (2021).
[48] J. D. Watts and R. J. Bartlett, "Economical triple excitation equation-of-motion coupled-cluster methods for excitation energies," Chem. Phys. Lett. **233**, 81 (1995).
[49] S. R. Stroberg, "IMSRG with flowing 3N operators," talk given at TRIUMF Workshop: Progress in *Ab Initio* Techniques in Nuclear Physics (2020).
[50] D. R. Entem and R. Machleidt, "Accurate charge-dependent nucleon-nucleon potential at fourth order of chiral perturbation theory," Phys. Rev. C **68**, 041001(R) (2003).
[51] S. R. Stroberg, https://github.com/ragnarstroberg/imsrg (2021).
[52] M. R. Strayer, W. H. Bassichis, and A. K. Kerman, "Correlation Effects in Nuclear Densities," Phys. Rev. C **8**, 1269 (1973).
[53] A. Tichai, J. Müller, K. Vobig, and R. Roth, "Natural orbitals for ab initio no-core shell model calculations," Phys. Rev. C **99**, 034321 (2019).
[54] J. Hoppe, A. Tichai, M. Heinz, K. Hebeler, and A. Schwenk, "Natural orbitals for many-body expansion methods," Phys.

Rev. C **103**, 014321 (2021).
[55] T. D. Morris, N. M. Parzuchowski, and S. K. Bogner, "Magnus expansion and in-medium similarity renormalization group," Phys. Rev. C **92**, 034331 (2015).
[56] N. Shimizu, T. Mizusaki, Y. Utsuno, and Y. Tsunoda, "Thick-restart block Lanczos method for large-scale shell-model calculations," Comput. Phys. Commun. **244**, 372 (2019).
[57] R. Roth, J. Langhammer, A. Calci, S. Binder, and P. Navrátil, "Similarity-Transformed Chiral NN+3N Interactions for the Ab Initio Description of ^{12}C and ^{16}O," Phys. Rev. Lett. **107**, 072501 (2011).
[58] S. J. Novario, G. Hagen, G. R. Jansen, and T. Papenbrock, "Charge radii of exotic neon and magnesium isotopes," Phys. Rev. C **102**, 051303(R) (2020).
[59] D. A. Varshalovich, A. N. Moskalev, and V. K. Khersonskii, *Quantum Theory of Angular Momentum* (World Scientific, Singapore, 1988).
[60] J. Suhonen, *From Nucleons to Nucleus: Concepts of Microscopic Nuclear Theory* (Springer, Berlin, 2007).
[61] A. Tichai, R. Wirth, J. Ripoche, and T. Duguet, "Symmetry reduction of tensor networks in many-body theory I. Automated symbolic evaluation of $SU(2)$ algebra," Eur. Phys. J. A **56**, 272 (2020).
[62] S. P. Pandya, "Nucleon-Hole Interaction in jj Coupling," Phys. Rev. **103**, 956 (1956).